LBL-3985
c.1

AN INVESTIGATION OF THE $Cu_xS/Cd_{1-y}Zn_yS$ HETEROJUNCTION: A POTENTIALLY LOW-COST, HIGH-EFFICIENCY PHOTOVOLTAIC ENERGY CONVERTER

Terry Michael Peterson
(Ph. D. thesis)

August 1975

Prepared for the U. S. Energy Research and
Development Administration under Contract W-7405-ENG-48

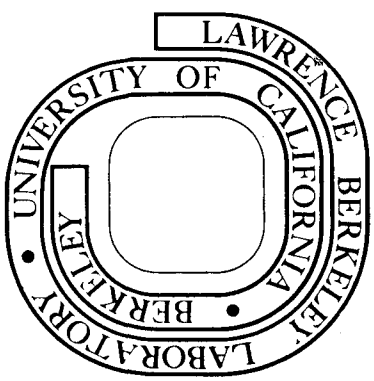

LBL-3985
c.1

DISCLAIMER

AN INVESTIGATION OF THE $Cu_xS/Cd_{1-y}Zn_yS$ HETEROJUNCTION:
A POTENTIALLY LOW-COST, HIGH-EFFICIENCY PHOTOVOLTÄIC ENERGY CONVERTER

Contents

AN INVESTIGATION OF THE $Cu_xS/Cd_{1-y}Zn_yS$ HETEROJUNCTION: A POTENTIALLY LOW-COST, HIGH-EFFICIENCY PHOTOVOLTÄIC ENERGY CONVERTER

Terry Michael Peterson

Inorganic Materials Research Division, Lawrence Berkeley Laboratory and Department of Materials Science and Engineering, College of Engineering; University of California, Berkeley, California 94720

ABSTRACT

Heterojunction photovoltäic cells of cuprous sulfide and cadmium-zinc sulfide ($Cd_{0.75}Zn_{0.25}S$) were made by dipping single crystal cadmium-zinc sulfide in an aqueous Cu^+ solution. For purposes of comparison, cells were also made of cuprous sulfide on single crystal cadmium sulfide and zinc sulfide. The cadmium-zinc sulfide, "mixed crystal", cells' properties were found to be superior to the CdS cells' in all respects, except short-circuit current density. In particular, they had higher power conversion efficiencies. It is argued that the higher efficiency of the mixed crystal cells together with the likelihood of their having greater stability than the CdS cell (because of lower copper diffusivity) makes them an attractive alternative to other photovoltäic cells for economical solar power conversion.

A theoretical model of the cuprous sulfide/II-VI semiconductor heterojunction is developed. The model is an extension of currently accepted models of such junctions incorporating explanations of (1) enhancement/quenching data found in two-beam experiments in terms of the rigid-band model of cuprous sulfide first proposed by B. J. Mulder; (2) the decrease in short-circuit current in djurleite-CdS cells, as compared to chalcocite-CdS cells, in terms of the movement of dislocation arrays required for lattice mismatch accommodation; and (3) the change in barrier height and spectral response of cuprous sulfide-$Cd_{1-y}Zn_yS$

heterojunctions, as the zinc fraction is increased, in terms of the change in electron affinity of the II-VI compound.

I. INTRODUCTION

A. Background

Recent changes in the long-standing situation of cheap sources of energy, the backbone of which was the low price of petroleum, have painfully focused public attention on a fact which far-sighted people, such as Farrington Daniels,[1] discovered decades ago: the resources on this planet required by industrialized human activity are finite. Furthermore, they are not "finite" in the abstract way a large lake from which a person takes one drink is finite, but finite in the concrete sense of a small canteen which must satisfy the thirst of that same person for an indefinite period.

The political and strategic motives of the "energy crisis" have been exposed; and the real problem is seen to be on the horizon rather than the doorstep. Nevertheless, a real problem exists and very few "long-term" solutions have been proposed. All of these involve the harnessing of the conversion of mass into energy during nuclear reactions. Those which are usually termed nuclear or atomic energy schemes seek to perform these reactions here on the earth. Nuclear fusion and the fast breeder fission reactor both promise to provide mankind with abundant supplies of energy for as long as he shall live. However, at this time, earth-born fusion power is hardly more than a glimmer in a physicist's eye, since even the most optimistic estimates place the date of its demonstrated feasibility decades in the future. On the other hand, the fast breeder reactor development program is encountering new technological problems faster

than solutions to existing problems can be found. An even more overriding concern to this author, however, is the fact that a concomitant circumstance of the proliferation of nuclear reactions of any type on the earth will be an absolutely incredible potential for self-destruction. When there is an alternative, it seems worse than foolish to accept the risk.

The alternative to the nuclear energy schemes is to make more efficient use of the sun, that fusion reactor which has always been the source of our energy. The technology for efficient solar energy utilitization already exists, in spite of its development having been hampered by the low regard in which most of those controlling research budgets have held it. The heat from the sun can be captured and used to heat or cool homes and buildings in ways which right now are competitive with more traditional methods on strictly economic grounds, as well as in terms of performance. Furthermore, the price/availability of petroleum does not have to change very much more, if at all, before production of electricity via solar-driven steam generators will be economically attractive.

Another way to harness solar energy is the "solar cell" which uses the photovoltäic effect to convert sunlight "directly" into electricity. This method has a certain aesthetic appeal because of its simplicity and straightforwardness. Unfortunately, all the current devices which perform this task are unsatisfactory for one reason or another. The two principal contenders (at least, up until the advent of the GaAs cell) are the silicon cell and the "cadmium sulfide" cell. The former has had over 10 years of extensive

development sponsored by the various space programs to provide an efficient, light weight power source for satellites; which has resulted in an efficient, but expensive, cell. So far the attempts at producing a Si cell at a "reasonable" cost have been disappointing. The cadmium sulfide cell has had less development, but appears to be marginal in terms of efficiency and stability.

The present work was undertaken in the hope that a more efficient and more reliable cell would be developed which still shared the cadmium sulfide cell's ability to be fabricated in a "thin film" form suitable to economical large scale production.

B. The Problem

The chief advantage of the so-called cadmium sulfide solar cell compared to the silicon solar cell is the demonstrated feasibility of fabricating the CdS cell in thin-film form suitable for economic production of very large area collectors. In almost all other respects the Cu_xS-CdS heterojunction* cell (as the cadmium sulfide cell is more properly called) is an inferior device to the traditional Si cell. It appears to be inherently of lower efficiency; and worse yet, for efficient operation it is required that the Cu_xS layer be very nearly stoichiometric chalcocite (Cu_2S), the least stable of the cuprous sulfides under normal terrestrial conditions.

---

*A comment on notation: In denoting a heterojunction, a slash will be used to indicate the configuration of the cell, e.g., Cu_xS/CdS = front-wall cell; unless the reference is generic, in which case a hyphen will be used.

The present investigation was launched as a result of the conjecture that one might possibly produce Cu_xS-based cells with improved stability by replacing the CdS with another n-type semiconductor. As the effects of crystal structure match, lattice parameter match, and electron affinity match became more fully appreciated, the project evolved into its present form. The main goals of this work are to demonstrate the feasibility of a Cu_xS-$Cd_{1-y}Zn_yS$ cell and to examine its properties in comparison with those of the conventional Cu_xS-CdS cell in order to further the understanding of both structures.

C. Prior Related Research

P. F. Lindquist[2] has published an excellent summary of the early work on the Cu_xS-CdS system. For the purposes of this work it will suffice to say that since the discovery of the "CdS" photovoltäic effect by D. C. Reynolds[3] et al. in 1954, the understanding of the device has evolved through several interesting, but erroneous, explanations (e.g., Refs. 3-7) into the present, generally--but not universally--accepted model, which is detailed and extended in Section II. The principle difference of the current model from earlier ones is in the recognition of the Cu_xS layer as the production center of the photocurrent, a mechanism apparently first proposed by Potter and Schalla.[8]

The discussion in the literature of ZnS and $Cd_{1-y}Zn_yS$ relevant to Cu_xS-$Cd_{1-y}Zn_yS$ junctions has been largely limited in the case of ZnS to recipes for doping single crystals[9] and forming ohmic contacts;[9-12] and in the mixed crystal case, to methods of preparation of single crystals.[13] There are several papers dealing with the physical,

optical, and electronic properties of ZnS or $Cd_{1-y}Zn_yS$ crystals (e.g., 14*-16) and thin films[17] which are of passing interest in connection with the Cu_xS-$Cd_{1-y}Zn_yS$ junction; and at least one paper by A. N. Georgobiani and V. I. Steblin[18] is devoted to the electroluminescence of Cu_xS-ZnS heterojunctions, but no mention is made of photovoltäic operation. To the author's knowledge, there is but one (guarded)reference to a $Cu_xS/Cd_{1-y}Zn_yS$ heterojunction photovoltaic energy converter which is found in the 1973 paper of Palz et al.[19] There, some results on a 10% ZnS cell are reported, including an increase in open-circuit voltage compared to the standard cell. However, the short-circuit current is said to be low.

Some workers[19,20] claim that the stability problems of the cadmium sulfide cell are solved; however, the maximum efficiencies claimed are still below 10%, which figure is generally held to be about the minimum necessary to make photovoltäic conversion competitive. (At lower efficiencies too much area is consumed by the collector, irrespective of the cost.) The use of $Cd_{1-y}Zn_yS$ instead of CdS will give an increase in open-circuit voltage of up to a factor of ~2, because of its lower electron affinity. At the same time, the short-circuit current density should at worst be unchanged, and may be increased because of the possibility of better lattice matching to the cuprous sulfide phase. Furthermore, the $Cd_{1-y}Zn_yS$ "mixed crystal" cell should possess greater inherent stability than the CdS cell,

*Of particular interest, is the result noted in Ref. 14 that the dark conductivity of as-grown crystals exhibits a sharp drop at about 20% ZnS.

since the mixed crystal with its smaller lattice parameter should resist the in-diffusion of copper ions better; and since it should prove possible to make efficient mixed crystal cells using the more stable cuprous sulfide phase called djurleite instead of requiring chalcocite as in the CdS cell.

II. THEORY

A. The Cu_xS/II-VI Band Diagram*

The heterojunction formed between cuprous sulfide and II-VI compounds such as CdS or, as in the present investigation, $Cd_{1-y}Zn_yS$ is not well understood theoretically at present. Indeed, one of the objectives of this work is to further the understanding of this kind of structure. The general theory of heterojunction operation as outlined by Sze[21] will be summarized here as a starting point in the development of a theory for the Cu_xS/II-VI heterojunction to explain its operation and predict its properties.

Figure 2.1a shows the energy band diagrams corresponding to two isolated semiconductors with no surface states and with differing band gaps E_g, electron affinities χ and types (p on left, n on right). If there were no interfacial electronic energy states to complicate the situation, the equilibrium band diagram, after these two semiconductors are brought into intimate contact, but still isolated from everything else (including light), would be as shown in Fig. 2.1b. Notice that the general there is a discontinuity in the bottom of the conduction band and the top of the valence band. The conduction band step equals the difference in the original electron affinities $(\chi_2 - \chi_1)$ and may be either positive, as shown, or negative. (This also fixes the valence band discontinuity, of course.) The electric displacement vector ($D = \varepsilon E$) must be continuous across the interface; therefore, unless the two materials have the same dielectric constant,

*The use of the slash (/) in "Cu_xS/II-VI" is not intended to denote cell configuration.

the slopes of the conduction and valence bands--being proportional to the electric field--will be discontinuous. (Of course, these infinitesimally sharp potential energy discontinuities are merely mathematical abstractions. A more realistic approach would be to smooth them out over some distance, perhaps even many lattice constants. Nature may not truely abhor a vacuum, but she finds discontinuities incomprehensible.) Solution of Poisson's equation with suitable boundary conditions yields the zero-bias widths of the depletion regions on either side of the metallurgical interface:

$$x_1 = \sqrt{\frac{N_2}{N_1}}\, x_0 \qquad x_2 = \sqrt{\frac{N_1}{N_2}}\, x_0 \tag{1a,b}$$

$$x_0 = \left[\frac{2\varepsilon_1\varepsilon_2 V_b}{q(\varepsilon_1 N_1 + \varepsilon_2 N_2)}\right]^{1/2} \tag{1c}$$

where N_i, ε_i are the net dopant concentration and permittivity of semiconductor i, q is the magnitude of the electronic charge and V_b($= V_{b1} + V_{b2}$) is the total barrier height ("diffusion potential"). One notices that Eqs. (1a,b,c) indicate that in a case such as the Cu_xS-CdS or Cu_xS-$Cd_{1-y}Zn_yS$ structures, where $N_1/N_2 \approx 10^3$ and $x_o \approx 100\text{Å}$, the extension of depletion region into the Cu_xS (semiconductor 1) is virtually zero.

One effect of energy states within the forbidden gap at the interface (interfacial states) is to shift the band edges at the interface up or down; and to decrease the depletion layer thickness on the p- or n-type side depending on whether the states are acceptor- or donor-like respectively. In particular, the presence of acceptor

states at the Cu_xS/II-VI interface will further decrease the depletion region in the copper sulfide.

Another effect of interfacial states, the presence of which is almost a certainty in the case where the lattice constants of the materials comprising the heterojunction are not identical, is the trapping and recombination of free carriers arriving at the junction. It has been suggested[22] that this effect of lattice mismatch accounts for a substantial part of the decrease in short-circuit current of Cu_xS/CdS cells which accompanies an increase in the copper deficiency of the Cu_xS.[23] (See also Appendix B.)

Interfacial states or other localized states near the interface have also been invoked to explain some of the reversible and nearly reversible changes in the I-V characteristics of Cu_xS-CdS cells after heat treatment.[24]

B. The Photo-Current

The mechanism of the production of photo-current in the Cu_xS-$Cd_{1-y}Zn_yS$ structure is analogous to that in a p-n homojunction such as the silicon cell. For a general discussion of the operation of a photovoltäic cell the reader is referred to Ref. 21, pt. IV, sec. 3.

In principle, of course, one can collect the minority carriers from either side of a heterojunction just as in the case of a homojunction. However, in conventional Cu_xS-CdS cells the bulk of the current is due to injection of electrons from the Cu_xS into the CdS. This is a consequence of two factors: (1) The conventional cell is of the front-wall type with the light incident on the Cu_xS. Therefore, photons energetic enough to be absorbed by the CdS are

too strongly absorbed in the Cu_xS to penetrate into the CdS. (2) The band gap of CdS (2.4 eV) is too wide to allow adsorption of most solar photons whose spectrum is approximately that of a black body at 5700°K whose maximum spectral intensity corresponds to a photon energy of 2.45 eV. At least in the case of front-wall $Cd_{1-y}Zn_yS$ cells the first factor still applies; and, in any case, the second factor carries even more weight since the mixed crystal has a larger band gap than CdS. Therefore, one can account for the observed (solar) spectral response of Cu_xS-CdS or $Cd_{1-y}Zn_yS$ cells quite well by calculating the electron injection current alone. This is shown in Fig. 2.2 taken from Ref. 22 where the response is calculated from the optical absorption constants of Cu_xS reported by B. J. Mulder[25] and compared with the spectral response measured by Palz et al.[23] The correspondence would be improved if the effects of cell series resistance had been incorporated into the calculation and if the djurleite response were corrected for interfacial recombination.

C. The Conduction Band Spike

A conduction band "spike", i.e., the condition where $\Delta E_c > 0$ as pictured in Fig. 2.1, has been proposed;[26] and several calculations based on such a model have been made[2,26,27] in order to explain some features of the behavior of Cu_xS-CdS cells. A refinement of these calculations has been carried out as part of the present investigation. The details of the method are discussed in Appendix A. The results are typified in Figs. 2.3 through 2.9. Figure 2.3 shows the transmission as a function of electron energy at a simple triangular potential with ΔE_c as a parameter. Figure 2.4 shows the average transmission

of a Maxwell-Boltzmann distribution of electrons incident on a triangular barrier as a function of the total depletion region thickness W when the barrier is 4 kT (0.1 eV) high. Notice that the transmission does not approach the classical transmission in the limit of large W. This is a result of the abrupt step at x = 0.

Figures 2.5 and 2.6 show the results of calculations to examine the effects of a discontinuity of the integrated transmission and determine how rapidly these effects diminish as the discontinuity is smoothed out. Figure 2.5 shows the effects of abrupt positive and negative steps in an otherwise constant potential. In Fig. 2.6 one sees that the reflection at a negative step and, hence, the non-classical reflection at a positive step is effectively eliminated when it has been spread out over about 12Å, approximately the wavelength of an electron with energy kT at room temperature.

The results shown in Figs. 2.7 and 2.8 were obtained using the potential shown in Fig. 2.9 wherein the unrealistic discontinuity of the triangular barrier is replaced with a ramp of width δ = 12Å and the depletion regions are made quadratic in x, corresponding to uniform doping. It is seen that these results do not differ markedly from the triangular barrier calculations, except that for large W the transmission approaches the classical value, just as one expects.

Notice that in both Figs. 2.3 and 2.7 the transmission is a monotonically increasing function of energy, having no maxima, unlike the case of the simple square barrier.[28] This property is a consequence of the fact that the barrier has no definite thickness and, therefore, there are no "resonant" energies for incident electrons.

(This fact seems to have escaped some workers (e.g., Ref. 27) whose graphs of transmission vs electron energy in some cases exhibit pronounced maxima because of the relatively small number of steps in their approximating potential.)

Figure 2.7 demonstrates quite clearly that, even in the case of a modest 0.1 eV barrier height, one sees no appreciable transmission unless the depletion region is less than about 200Å thick. However, measurements of junction capacitance during illumination[2,26,29] show that the depletion layer is $\gtrsim$1000Å. Also, low-temperature measurements[2] yield maximum open-circuit voltages of about 0.65 V, whereas the value should be closer to 1.2 V if there were a conduction band "spike". Furthermore, if ΔE_c were already greater than zero, the addition of zinc to the cadmium sulfide, further decreasing its electron affinity, would have disasterous effects on device performance; which is decidedly not the case (see Section V). Therefore, it seems the existence of a positive ΔE_c at the Cu_xS-CdS junction is an untenable hypothesis.

D. The Rigid Band Model of Cu_xS

The rigid band model of Cu_xS proposed by B. J. Mulder[30] starts with the assumption that the electronic energy states in chalcocite and djurleite (and digenite) are essentially the same. The justification for this assumption lies in the similarity of the optical absorption constants of these materials. Its plausibility can also be argued on the basis of the observation that the more copper deficient phases are derived from chalcocite essentially by removing copper ions from interstitial sites in the sulfur sublattice. Then,

to explain the disappearance of the indirect absorption edge at 1.2 eV in the chalcocite-djurleite transformation, the band structure shown in Fig. 2.10 is proposed.

This structure also seems to account for the well-known non-linear effects observed in heat-treated (i.e., oxydized) CdS cells, as explained in detail in Ref. 31, and outlined here. There are two, complementary effects: (1) enhancement of long wavelength response in the presence of short wavelength illumination, and (2) quenching of short wavelength response by simultaneous long wavelength light. These effects are usually distinguished by means of chopping one light beam and observing the ac component of the short-circuit current.[7,26] These effects have been attributed to interfacial states and trapping levels in the CdS depletion layer.[6,7,29] However, this explanation would seem to ignore the fact that the total (ac + dc) current usually increases when the total light intensity increases.* The quenching/enhancement is with respect to one or the other of the components of the current.

In terms of the rigid band model these effects are thought to be due to the increased transition rate between the conduction and indirect valence band in djurleite, because of stimulated emission in the presence of long wavelength light (i.e., where $h\nu \approx E_{gi}$). The observation of enhancement or quenching then depends on the details of

*There is, of course, no intention here to deny there are interfacial states. Indeed, Fahrenbruch and Bube[9] have identified thermally and optically stimulated electrical effects, independent of the quenching/enhancement effect, which seem well accounted for by localized states at or near the junction.

the experimental set-up, i.e., whether long or short wavelength light is chopped and whether one measures the ac or dc component of the current. The effect is absent in chalcocite because the Fermi level lies well above the direct valence band maximum and a population inversion of the conduction band with respect to the indirect valence band cannot be established.

III. EXPERIMENTAL METHODS AND APPARATUS

A. Sample Preparation

The single crystal starting materials for this work were all obtained from the Eagle-Picher Company. The ZnS crystal was purchased as a single, 10 g piece which was then oriented by X-ray diffraction and sliced with a carborundum saw perpendicular to the c-axis. The CdS was oriented in the same way, having been cut with a diamond-impregnated wire saw. The $Cd_{0.75}Zn_{0.25}S$ (nominal) crystal (a gift from Eagle-Picher) was X-ray oriented in the same way as the ZnS and cut into slices on a diamond saw ("Isomet" low speed saw). The slices obtained were 5-10 mm in diameter and 1-2 mm thick, except for some of the CdS slices which were slightly larger in diameter.

All three kinds of crystal were doped to increase their conductivities in essentially the following manner:[9] A single crystal slice was was placed in a quartz ampoule together with a small quantity ($\lesssim$1 g) of the dopant metal, zinc in the ZnS case and cadmium in the others. The ampoule was evacuated with a mechanical pump and back-filled with argon or argon + 2% H_2 at least three times and finally evacuated and sealed. Then the ampoule was placed in a tube furnace and fired for 120-140 hr. The temperature of the firing depended on the crystal, 950°C for ZnS and 800° for CdS and the mixed crystal. It was found during the ZnS work that one must not remove the crystal directly from the furnace, as this apparently quenches in too many vacancies so that the crystal is entirely compensated. A successful procedure seems to be to turn off the furnace and allow the crystal to slowly (~2 hr) cool to about 400°C.

Several attempts were made to introduce zinc into a CdS crystal by diffusion at various temperatures in the manner just discussed. The results were very unsatisfactory since, in every case, the influx of Zn was accompanied by the propagation of microscopic cracks into the crystal. Conversely, it was found possible to diffuse Cd into a ZnS crystal, but the process is exceedingly slow (~10% CdS at a depth of 75 μm after 120 hr at 950°C).

After doping, the samples were polished on both sides with the final lapping being done with a 1.0 μm diamond compound. After this step, it was found that all of the crystals contained various microscopic defects, principally faceted voids or bubbles. It is not known if they were all present before the doping process, but they were distributed in such a way as to suggest they were initiated by changes in conditions during growth rather than during the doping process; i.e., their position did not seem to be related to the slice geometry, but rather to the original crystal shape.

Ohmic contact was made to one side of the CdS and $Cd_{0.75}Zn_{0.25}S$ polished crystals by pressing dots of indium in place at room temperature; placing the crystal in a glass drying dish, which was covered while flushing with argon; and firing in a 400°C muffle furnace for 10 min (cf Ref. 12). The current-voltage linearity of these contacts was checked at room temperature and found to be very good. The stated procedure should yield good contacts to ZnS as well; however, the ZnS samples used had already been given contacts via a similar, earlier process[11] wherein an In-Ga amalgam is fired-on for a few minutes at 475°C and annealed several minutes at 400°C in a

flowing atmosphere of dry N_2. These contacts were also quite good at room temperature.

The ZnS samples were then mounted in a resin compound with the side opposite the ohmic contact exposed and were repolished. In some cases a gold blocking contact was vacuum evaporated on the exposed face for resistivity measurements (see Section IV-B). Otherwise the exposed face was etched in HCl solution and a Cu_xS layer was formed by vacuum depositing CuCl and heating at ~100°C for 2 hr in an argon-filled vessel. (The reason this method was employed instead of the solution dip described below was only that the proper techniques for maintaining the cuprous ion solution for the necessary length of time in the ZnS case were not known until later. It is now felt that the dipping method could also be used.) The remaining CuCl was washed off with ethanol and a cotton swab. Finally, contact was made to an edge of the Cu_xS with conductive silver paint. Thus, the ZnS cells are "front-wall" cells, the light being incident on the Cu_xS.

The CdS and mixed crystal samples were formed into "back-wall" cells similar to those described by Gill.[26] The crystals were masked by painting all but a small area (approximately opposite the ohmic contact dots) with edge protecting lacquer (H. Struers Chemiske Lab.). Then they were dipped in a Cu^+ solution for 2 hr. The solution recipe and dipping procedure followed those of Lindquist[5] quite closely (being far the most successful of those tried). In particular, 10 g of KCl, 3.5 g of $NH_2OH \cdot HCl$ and 5 g of CuCl were add to 250 ml

of water which had been boiled with argon bubbling through it for at least one half hour. The pH was not adjusted by the addition of HCl. The undissolved CuCl was grey-white and the solution was almost perfectly clear, becoming a very pale green by the end of the 2 hr dip. The samples, on a small glass dish, were added to the small glass washing dish containing the Cu^+ solution. The washing dish was placed inside a pre-warmed desiccator jar (without desiccant) and both were flushed with argon. A watch glass was put over the solution container and the desiccator was flushed again with Ar and closed. The assembly was placed in an oven at a nominal 90°C; however, the temperature control of the oven was not very good and the inside air temperature varied about ±5°C. The actual solution temperature was not determined. After the dip; the samples were quickly washed in water and ethanol; and the maskant was removed with perchloroeylene. The Cu_xS side of the cell was painted with silver paint which acted both as contact for the Cu_xS and glue to hold the sample to an aluminum substrate. (Except for cell #C8-16 which was not mounted on a substrate.) To complete the cell, Al wires were attached to the substrate and In contacts.

B. Electron Microprobe Measurements

A Materials Analysis Company electron microprobe was used[32] to examine the mixed crystal for variations in Zn to Cd ratio. These were suspected because of noticable spatial variations in optical properties, i.e., color and index of refraction. The microprobe data was reduced to concentrations by means of the computer program MAGICIV.[33]

C. Current-Voltage Characteristics

Cell I-V characteristics were determined with a Tektronix Type 502A oscilloscope and a Waveforms 401H sine wave generator (usually operated at 4 Hz) in the circuit illustrated in Fig. 3.1. Illumination was provided by means of an American Optical microscope lamp powered by a variable DC supply. Also used were various Kodak filters. Occasionally, the apparatus was moved near a window and the cell was tested in sunlight.

D. Spectral Response Characteristics

The spectral response measurements were carried out with the set-up illustrated in Fig. 3.2. The quartz-halogen lamp supply was always adjusted for a lamp current of 6 amperes. An Oriel Model 7240 monochromator with a 750 mm blaze, 1200 1/mm grating, and 1.8 mm slits which give a 12 nm bandpass was used. The monochromator output vs wavelength was determined with a Hewlett-Packard Model 8330A radiant flux meter with an 8334A thermopile detector. The short-circuit current was measured with a Keithley 602 electrometer. In the open-circuit mode the load on the cell was >10''Ω; and in the short-circuit mode the voltage drop was <1.0 mV. The flux meter readings were then used to normalize the short-circuit current to constant incident intensity, assuming the short-circuit current to be proportional to incident intensity.

IV. EXPERIMENTAL RESULTS

A. Electron Microprobe Measurements

As was suspected from the observation of striations in the index of refraction and in the color of the mixed crystal after doping, the electron microprobe scans showed local variations in the Cd/Zn ratio. A plot of one of these scans appears in Fig. 4.1 where it is seen that there is both a long range change and a superimposed periodic change with a wavelength of about 0.8 mm. The surface scanned was a basal plane; and the smaller the "position" coordinate, the closer the beam was to the original crystal surface (i.e., the surface before slicing). It was also noted that the striations were somewhat correlated with the distribution of the other defects observed (bubbles/voids).

B. Current-Voltage Measurements

1. ZnS Cells

The current-voltage (I-V) characteristics of two kinds of barrier were studied. In connection with the effort to dope the ZnS crystals to a sufficiently high conductivity to be useful in heterojunction studies, gold or aluminum Schottky barrier contacts were used in addition to the In-Ga ohmic contacts. The Au contact characteristics were stable, with a barrier height of about 2 volts. Aluminum contacts were first used, but discontinued because they were less stable; the barrier tended to increase with time. This result was thought possibly to be due to the formation of an MOS-type structure.

The slope of the forward-biased part of the I-V curve of the Au Schottky barriers was used to give an indication of the dopant

level in the ZnS. In the best cases, the dopant concentration was found to be about 2×10^{16} cm^{-3}. (This was checked with a plot of junction capacitance vs reverse bias which gave a comparable result.) The evidence of the need for slow-cooling of the sample is shown in Fig. 4.2 which shows the I-V characteristics of two Schottky barrier samples (in this case the blocking contact is provided by silver conductive paint) made from ZnS samples given the same doping treatment, except that one was allowed to cool slowly to 400°C and the other was removed from the 950°C furnace directly to the ambient. One sees that the rapidly cooled sample exhibits no measurable dark conductivity, and even the photoconductivity is poor. However, the slow-cooled specimen shows good photoconductivity and exhibits substantial (for ZnS) dark conductivity.

The Cu_xS/ZnS junction exhibited some interesting I-V characteristics. These heterojunctions appear to consist in general of a mixture of two "pure" types having barrier heights of about 1 volt and 1.5 volts respectively. With heat treatments or even aging in the laboratory they gradually move toward the pure 1.5 volt type. In a few cases the as-made barrier was of the pure 1.0 volt type. One of these is shown in Fig. 4.3a where one sees the I-V characteristics of cell #1Z9-26 under a focused microscope lamp. The opposite extreme is the cell of the 1.5 V type whose I-V characteristic is shown in Fig. 4.3b. This was obtained from cell #1Z4-12 after some mild heat treatments (5 hrs total at 100°C) and aging in the laboratory for 35 days. In the as-formed condition, cell #1Z4-12 had a typical Cu_xS/ZnS cell I-V trace; i.e., a mixture of the 1 and 1.5 V types with a double

"knee". This is illustrated in Fig. 4.3c. This cell also had the highest sunlight conversion efficiency of any of the Cu_xS/ZnS cells made. The efficiency computed from Fig. 4.3c is 0.3%.

2. CdS Cells

The I-V characteristic of the CdS/Cu_xS cells made here are in substantial agreement with those obtained for non-heat treated cells by Gill.[26] There is no "cross-over" of the light and dark characteristics, such as is found in most Cu_xS-CdS cells where a heat treatment is incorporated into the manufacturing process. Figures 4.4a and 4.4b show the I-V characteristics of CdS/Cu_xS cell #C8-16 in sunlight and focused microscope lamplight respectively. In both 4.4a and 4.4b the order of increasing I_{SC} is (1) dark, (2) $\lambda > 700$ nm, (3) $\lambda > 630$ nm and (4) unfiltered sunlight/lamplight. The short-circuit current in sunlight (~100 mw/cm^2) is 2 mA/cm^2; V_{oc} = 0.2 V; and the conversion efficiency is about 0.15%. These values appear very similar to values for non-heat-treated cells of similar construction reported by others.[2,26,33]

3. Mixed Crystal Cells

In contrast to the CdS cells, the as-formed mixed crystal cells did exhibit cross-over of the light/dark I-V characteristics, as can be seen in Figs. 4.5a and 4.5b. The illumination conditions used to obtain these characteristics were, as far as possible, identical to those of Figs. 4.4a and 4.4b. The short-circuit current of the mixed crystal cell in sunlight was about 60% of that of the CdS cell of Fig. 44a (1.35 mA/cm^2); while the open-circuit voltage was 2.7 times higher. The power conversion efficiency was 0.34%, or

a little more than twice that of C8-16. There is some uncertainty about the comparison of the short-circuit current densities (J_{sc}) of the mixed crystal and CdS cells. The effective junction areas were determined from micrographs of the cells and the areas covered by the ohmic contacts were not included; however, the fraction of the total junction covered by the contacts was larger in the CdS case. Therefore, if light scattered behind the contacts made a significant contribution to the total current, the figures for the short-circuit current densities of the two cells would be closer. In fact, if the total junction area is used, the J_{sc}'s differ only by about 20%.

C. Spectral Response Measurements

1. ZnS Cells

Figure 4.6 shows the short-circuit current vs wavelength of incident light normalized to constant intensity for Cu_xS/ZnS cell #2Z8-13. One sees that even though this is a front-wall cell where the light must pass through the Cu_xS layer (except near the edges of the junction), the measured response appears to have been totally due to absorption in the ZnS; i.e., there was no measurable response at wavelengths longer than those corresponding to photons of energies equal to the band gap of ZnS. Also, the current readings were stable, showing no transient effects.

2. CdS Cells

The short-circuit current response shown in Fig. 4.7 of cell #C8-16 is very typical of non-heat treated spectral response characteristics of CdS/Cu_xS cells of this construction (cf Refs. 2, 26, 34).

The response extends beyond 900 nm; and is relatively constant down to about 550 nm where the light starts to be absorbed by the CdS before it can penetrate to the junction. Also typical of such cells, there were no transient effects in the response.

3. Mixed Crystal Cells

The spectral response of cell #M8-16 is shown in Fig. 4.8. The larger band gap of the $Cd_{0.75}Zn_{0.25}S$ compared to CdS allows the short wavelength response to extend to less than 500 nm. The response is not as uniform from 550 nm to 900 nm as in the CdS case. Also, there were some transient response effects similar to the self-enhancement and self-quenching described by Gill[26] as occurring in heat treated CdS/Cu_xS cells. The initial response would either gradually decrease or increase to a steady-state value depending on the wavelength of the incident light. For cell #M8-16 the change was negative for $\lambda \gtrsim 900$ nm and positive for shorter wavelengths. The magnitude of the effect observed here was smaller than that reported for the heat treated CdS case, however, being at most only about 10% of the total current. In the region $1000 \text{ nm} < \lambda < 1100$ nm the slopes of the mixed crystal and CdS crystal cells' characteristics are about the same (about a decade change in I_{sc} in 65 nm).

V. DISCUSSION OF EXPERIMENTAL RESULTS AND OF AGREEMENT OF EXPERIMENT WITH THEORY

A. Mixed Crystal Inhomogeneity

The inhomogeneities found in the $Cd_{0.75}Zn_{0.25}S$ crystal used for this study point up the need for very careful control of the crystal growth or thin-film deposition conditions used in the fabrication of mixed crystal cells in any future work. The areas showing the least amount of variations in optical properties were chosen for junction formation; however, it is unknown what effects the inhomogeneities which were present near the junction had on the device characteristics. Since considerations of lattice parameter match and electron affinity match at the heterojunction suggest that there will be an optimum Cd-Zn ratio (perhaps, several--one for each cuprous sulfide phase), it is likely that efficient Cu_xS-$Cd_{1-y}Zn_yS$ cells will require extremely close control of mixed crystal growth. This task will, perhaps, be easier in the manufacture of thin film cells where the $Cd_{1-y}Zn_yS$ layer will be doped as it is formed by suitable control of the constituent vaporization rates.

B. Cu_xS/ZnS Cell Measurements

The measurements carried out on Cu_xS/ZnS cells shed some light on two aspects of the nature of Cu_xS-CdS heterojunctions. First, the behavior of the Cu_xS/ZnS barrier height supports the rigid-band (RB) model[30] of chalcocite/djurleite in the following way: one hypothesis of the RB model is that the conduction band remains nearly unchanged in the chalocite-djurleite transformation and that the increase in apparent band gap is due to the lowering of the fermi level to the top of a second (direct) valence band, as shown in Fig. 5.1

(see also Fig. 2.10). It can be seen in Fig. 5.1 that this change in the fermi level will be accompanied by an increase in the barrier height approximately equal to the fermi level shift. Indeed, it is observed that heat treatments or aging in normal laboratory conditions, both of which should tend to promote a loss of copper in the Cu_xS phase, are accompanied by such an increase in barrier height. It should also be noted that a shift of the conduction band (i.e., with respect to the ZnS conduction band) to accomplish the required change in band gap is unlikely to have the same effect on the barrier, since there then could be current flow by tunneling through interfacial states for forward biases greater than the original barrier voltage.

The second feature of the Cu_xS/ZnS cells of importance to the understanding of the Cu_xS-CdS cell is the total lack of response at wavelengths longer than those absorbed by ZnS. This suggests the photovoltaic response mechanism in the Cu_xS/ZnS system is different from the CdS case. It is known that the electron affinity of ZnS is about 1 eV less than that of CdS.[9] Therefore, there is almost certainly a conduction band spike at the Cu_xS-ZnS interface like the one described in Section II as having been proposed for the Cu_xS-CdS junction. Hence, the lack of long-wavelength response corroborates the predictions of the calculations explained in Appendix A and illustrated in Figs. 2.3 through 2.9; and it casts further doubt on the existence of a spike in the CdS case where there is always some response at wavelengths greater than those absorbed in the CdS.

C. CdS/Cu_xS Cell Measurements

The purpose of fabricating CdS/Cu_xS cells during this work was largely to verify that the procedures being followed yielded the expected results in this relatively well-studied system. The spectral response data and I-V characteristic behavior were quite typical of the similar cells studied by the Stanford workers.[2,26,34] The performance of these cells is rather poor compared to normal thin film Cu_xS/CdS cells which have about twice as high V_{oc} and about a factor of 10 higher I_{sc}. It is thought these differences are due to the high series resistance of cells of the construction used here.

D. Mixed Crystal Cell Measurement

The experimental results on the mixed crystal cells seem comprehensible in the context of the theoretical model developed in Section II. The rigid-band model together with considerations of electron affinity and lattice parameter matching at heterojunctions lead one to expect that the $Cd_{1-y}Zn_yS/Cu_xS$ cell performance characteristics will be similar to those of the CdS/Cu_xS sell. More specifically, one expects that the addition of Zn to CdS will bring about an increase in both open circuit voltage and short-circuit current. The former is because the Zn will increase the electron affinity on the II-VI side of the junction, thus increasing the barrier height; and the latter, because the substitution of Zn for Cd causes a reduction in the lattice parameter, allowing a closer match to the Cu_xS lattice (either chalcocite or djurleite), which decreases the equilibrium number of misfit-accommodation dislocations, and with them, the number of trapping-recombination states near the junction. (See Appendix B

for a discussion of this effect.) Furthermore, the rigid-band model requires that the sunlight produced short-circuit current of a djurleite cell should not differ much from that of a chalcocite cell. This is because the loss in long wavelength response observed in monochromatic response characteristics of djurleite cells does not exist in the presence of simultaneous short-wavelength illumination.[26] Therefore, when the number of misfit accommodation dislocations in the djurleite cell has been reduced by tailoring the lattice parameter of the $Cd_{1-y}Zn_yS$, the currents should be nearly equal.

The expectation of a higher V_{oc} was certainly fulfilled by the mixed crystal cells, since they produced open-circuit voltages about 50% higher than those normally found at room temperature for CdS cells and more than twice that of the CdS cells of the same construction. While the uncertainty about the true effective junction area, discussed in Section IV-B-3, does not permit a reliable comparison of the short-circuit current densities of the CdS and mixed crystal cells; the results do tend to support the prediction of equal current.

The spectral response behavior of the mixed crystal cell is also easily accounted for in the model of Section II. The general shape of the response curve (Fig. 4.8) suggests that the heterojunction on the $Cd_{0.75}Zn_{0.25}S$ crystal is made with a mixture of chalcocite and djurleite because it lies midway between the shapes of the curves calculated for chalcocite and djurleite back-wall cells from absorption data (see Ref. 31). At the long-wavelength end it is falling at the same rate as the CdS/Cu_xS response curve which is a chalcocite response. (This is actually quite revealing, since I_{sc} is proportional to the absorption constant at the long-wavelength

extreme of a back-wall cell response characteristic. Therefore, identical wavelength dependence of the response implies identical absorption constants.) As the wavelength decreases in the region 500 nm < $\lambda \lesssim$ 900 nm, the mixed crystal cell response increases as the djurleite areas of the junction contribute more current and the chalcocite response is nearly constant (cf Figs. 4.7 and 4.8). This interpretation also accounts for the relatively weak self-enhancement/quenching observed in the mixed crystal cell. If one assumes, as suggested in Ref. 31, that the enhancement/quenching effects arise whenever djurleite is present in the cell; then the presence of some djurleite areas will give rise to some enhancement/quenching.

The cross-over of the light and dark I-V characteristics shown in Fig. 4.5 seems to be of a different nature than that reported in heat-treated CdS cells (e.g., Ref. 26) in that there is no shift of the barrier height. Gill's[26] heat-treated "cell #1" exhibits a dark or long-wavelength-lit barrier of about 1 V and a barrier of about 0.4 V under white or short-wavelength light. (Ref. 26, Fig. 4.2, p. 47.) Whereas, the as-formed mixed crystal cell studied here exhibits an increase in forward conductance with no change in V_{oc}. It seems likely that this is due to the photoconductivity of the mixed crystal and is not directly related to the properties of the heterojunction itself.

VI. CONCLUSIONS AND SUGGESTIONS FOR FUTURE WORK ON THE $Cd_{1-y}Zn_yS$ SYSTEM

A. Feasibility of the $Cd_{1-y}Zn_yS$-Cu_xS Cell

The results presented here demonstrate not only that the mixed crystal cell is a feasible alternative to the CdS cell, but that it is potentially both more efficient and more stable than the CdS cell. The feasibility of the $Cd_{1-y}Zn_yS$-Cu_xS cell is demonstrated by the facts that the cells were made and were found to have properties consistent with those predicted by the theoretical model presented. Their potential for greater efficiency than the CdS cells is due to their larger open-circuit voltage with little or no loss in short-circuit current density. It should be stressed that the valid comparison of efficiencies is between the various cells of the single crystal type made in this study and in similar studies,[2,26,34] not between these cells and thin film cells. This is because the factors (mainly series resistance) which limit the performance of the single-crystal back-wall cells are common to both the CdS and mixed crystal cells; and therefore, a thin-film mixed crystal cell should show roughly the same proportional increase in performance over the single-crystal cell that its CdS relative does.

Their potential for greater stability stems partly from the possibility of making efficient cells using the more stable (with respect to oxidation) djurleite phase of cuprous sulfide instead of being constrained by lattice matching to using chalcocite. Another factor leading to increased stability is the smaller lattice parameter

of the mixed crystal compared to CdS. This factor decreases the diffusivity of copper ions, which is so high in CdS as to cause device degradation at moderate temperature, so that the mixed crystal devices will be more resistant to damage from over-heating.

B. Summary of the Model of the Cu_xS/II-VI Heterojunction

The main points of the model believed to describe the observations of all the Cu_xS/II-VI heterojunctions reported here are as follows: (1) The photo-current is largely due to absorption in the cuprous sulfide, except in those cases (e.g., Cu_xS-ZnS) where the electron affinity of the II-VI compound is less than that of the Cu_xS, causing the existence of a conduction band "spike." (2) The conduction band "discontinuity" is negative (from the point of view of electrons arriving at the junction from the Cu_xS side) in Cu_xS-CdS heterojunctions; and becomes less negative with the addition of Zn on the II-VI side. At some Zn concentration, the step will be zero; and then, positive with larger Zn content. A positive step of any greater height than ~kT is disastrous to the transmission of electrons from the Cu_xS. (3) The band structures of chalcocite and djurleite (and possibly digenite) are essentially the same, having a single conduction band minimum and two valence band maxima--one directly below the conduction band minimum ~1.8 eV, and one indirectly below ~1.2 eV (see Fig. 2.10). The difference between the two phases is that in chalcocite the fermi level lies near the top of the indirect valence band and in djurleite it is near the top of the direct valence band which means the indirect band is nearly empty. This empty valence band is the cause of the quenching/enhancement effects found in

djurleite-containing cells. (4) Other effects not studied here, such as the shift in barrier height with illumination in heat treated CdS cells and the thermally restorable optical degradation (TROD) of CdS cells observed by Fahrenbruch and Bube,[29,34] are thought to be a result of the massive number of interfacial states accompanying the large number of misfit accommodation dislocations at the Cu_xS-CdS junction; or a result of the localized states introduced in the CdS by the copper ions in the "tail" of the diffusion front which formed the junction.

C. The Nature of the Cu_xS-CdS Cell

The present investigation, although not aimed directly at the Cu_xS-CdS heterojunction, as led to some clarification of the nature of that device. The first point is that the existence of a conduction band spike has been ruled out. The transmission probability calculations described in Section II, the observed spectral response of Cu_xS/ZnS cells in which there is thought to be a spike, and the high efficiency of the mixed crystal cell all indicate that there can be no such spike at the Cu_xS-CdS heterojunction.

Another observation of this study which has bearing on the Cu_xS-CdS system is the formation of djurleite areas during the junction formation on $Cd_{1-y}Zn_yS$ crystals under conditions identical to those yielding all-chalcocite layers on CdS. This finding supports the view that the extra interfacial energy necessary to nucleate djurleite on CdS because of its greater lattice mismatch is sufficient to inhibit its formation even when the Cu^+ activity is too low to make chalcocite the stable phase. This nucleation mechanism is

because, when the chalcocite subsequently transforms to djurleite, the resulting misfit accommodation dislocation array ends up in a field-free region and acts as an efficient recombination center to degrade device performance (see Appendix B and Ref. 22).

The fact that self-enhancement/quenching of the photocurrent was observed in the mixed crystal cell also tends to substantiate the hypothesis that the origin of these effects is the empty indirect valence band in djurleite. This is so because the mixed crystal cells were treated exactly as were the CdS cells which exhibited no enhancement/quenching phenomena. Therefore, the mixed crystal cells should not have suffered greater diffusion of copper to form a compensated layer, which is the kind of structure supposed in other explanations of these effects.

D. Suggestions for the Direction of Future Work

While the results presented in this work strongly support the use of a $Cd_{1-y}Zn_yS$-based cell in place of the current CdS-based type, there are several points of interest which have remained unsettled. The first of these is the question of what Cd-Zn ratio will produce the best cells, both in the sense of highest efficiency and of greatest stability. Secondly, is it possible--or desirable--to form homogeneously chalcocite or djurleite layers on the mixed crystal? Finally, one must make thin-film cells in order to verify that the gains in performance found in Cu_xS/CdS thin film cells as compared to the single crystal laboratory CdS/Cu_xS cells can be obtained in the mixed crystal case.

ACKNOWLEDGEMENTS

Perhaps the most pleasant task connected with the writing of this thesis is that of preparing this section; to acknowledge the help I have received in performing the work presented herein. First, I am indebted to Professor Jack Washburn without whose wise council and whole-hearted support this project could not have been completed. My thanks also to Professor Marshal Merriam, not only for his encouragement and advice during this work, but also for having initially sparked my interest in solar energy conversion. I am grateful to Professor Lee Donaghey for his continued interest in this project and for the helpful discussions we have had during its progress. I wish also to extend my sincere, heart-felt appreciation to the entire staff at the Inorganic Materials Research Division; each one of whom has, at some point or another in my stay here, been able to help my progress; any everyone of whom has done so with the friendly cooperation which has made working here such a great pleasure.

This work was done under the auspices of the U. S. Energy Research and Development Administration.

APPENDIX A. ON THE NUMERICAL CALCULATION OF QUANTUM MECHANICAL TRANSMISSION COEFFICIENTS FOR ARBITRARY BARRIER POTENTIALS

Since the time-independent Schrödinger equation in one dimension

$$-\hbar^2/2m(d^2\psi/dx^2) + V(x)\ \psi = E\psi \qquad \text{(a)}$$

is only ammenable to analytical solution for quite simple potentials V(x); and since the WKB approximation method usually invoked for more complicated potentials is not valid for the cases of interest, i.e., transmission of the order of unity; a numerical approximation scheme to find the transmission probability T(E) of an electron with energy E incident on an arbitrary potential barrier V(x) has been devised.[1] The method involves approximating V(x) by a piece-wise constant potential $V_i(x_i)$, $1 \leq i \leq N$, where N is a "large" number; and relating the coefficients of the wave functions on the incident and far sides of the barrier via a complex-matrix multiplication of the coefficients of the intervening wave functions.

The matrix relating the coefficients of the solution to (a) at a step in an otherwise constant potential

$$V(x) = \begin{cases} V_1 , & x < a \\ V_2 , & x > a \end{cases} \qquad \text{(b)}$$

is given by Merzbacher[2]

$$\underset{\approx}{A} = \frac{1}{2}\begin{bmatrix} (1+\delta)\exp(-ia(k_1 - k_2)) , & (1-\delta)\exp(-ia(k_1 + k_2)) \\ (1-\delta)\exp(+ia(k_1 + k_2)) , & (1+\delta)\exp(+ia(k_1 - k_2)) \end{bmatrix} \qquad \text{(c)}$$

where $\delta = k_2/k_1$ and $k_j = (2m(E - V_j))^{1/2}$. This matrix is further defined by the relationships

$$\underset{\sim}{C}^{-} = \underset{\approx}{A}\,\underset{\sim}{C}^{+} \tag{d}$$

and

$$\psi^{\pm}(x) = \underset{\sim}{C}^{\pm}\begin{pmatrix}\exp(ikx)\\ \exp(-ikx)\end{pmatrix} \tag{e}$$

where +,- refer to $x > a$ and $x < a$ respectively. Evidently, one can apply Eq. (d) successively at each step in a piece-wise constant potential to obtain

$$\underset{\approx}{A}_{tot} = \prod_{i=1}^{N} \underset{\approx}{A}_i \tag{f}$$

where $\underset{\approx}{A}_{tot}$ is the matrix relating the coefficients of the wavefunctions on the two sides of the barrier and the $\underset{\approx}{A}_i$ are matrices of the form (c) at each of the steps in $V_i(x_i)$. If N is made sufficiently large, the width and height of each step (i.e., the deviation of V_i from V) becomes small compared to the wavelength and energy, respectively, of the electron and is reasonable to expect that the behavior of an electron incident on the barrier $V_i(x_i)$ would not differ markedly from that of an identical electron incident on the barrier V(x). Then if $\underset{\sim}{C}^{+}$ in Eq. (d) is made equal to (1,0), one can easily verify that the overall transmission probability is given by

$$T(E) = \frac{\rho_N v_N}{\rho_{incid} v_1} = \frac{|\psi_N|^2 k_N}{|\psi_{incid}|^2 k_1} = 1/|A_{11}|^2 \cdot \frac{k_N}{k_1} \tag{g}$$

Figure A.1 shows the FORTRAN FUNCTION T(E) which performs the procedure outlined above. The argument ENERGY of T is taken to be in units of kT (=0.025 eV) and is converted to electron volts after first checking to see that it is not "zero" ($<10^{-10}$) in which case the transmission is set to zero. All other energies are in electron-volts and all distances in angstroms. Within T; XL and XU are the starting and final positions (in Å) for which the transmission probability is to be found, NMAX is the largest number of steps to be allowed, and N is the number of steps used in the approximating function $V_i(x_i)$ (array VI). Whenever T is called while N = 0 (actually while N is any value different from the previous call), N and the arrays XI and VI are recalculated such that no step is both wider than DX and higher than DVMAX (typically 0.5Å and 0.001 eV respectively). Sample values of XI and VI (~1/15 of the total number) are printed as a check that everything is working right. Then, starting at statement 1000, the matrices A_i (array CA) are calculated and the cumulative product

$$\prod_{l=1}^{N} A_i$$

is stored in array CT. Finally, $1/|A_{11}|^2_{tot}$ is calculated, and multiplied by $|k_N|/|k_1|$.

An upper limit of 2000 has been imposed on N by the DIMENSIONS statement defining VI and XI. This can easily be increased; however, checking the numerical calculations with analytic solutions for simple potentials, e.g., the triangular barrier which involves Airy functions; and by changing DX and DVMAX has shown that larger N's are not necessary to achieve relative accuracies of about 1%.

1. After working this method out, it came to my attention that it is a fairly common procedure in some circles (Professor L. Falicov, private conversation). Even more recently I have become aware of G. H. Hewig's similar, although less accurate calculations, cf Ref. 4.
2. E. Merzbecher, Quantum Mechanics (John Wiley & Sons, Inc., 1961), p. 92.

APPENDIX B. ON THE EFFECT OF MISFIT ACCOMMODATION DISLOCATION ARRAYS IN Cu_xS/II-VI HETEROJUNCTIONS

The purpose of this appendix is to set forth an outline for the reader's convenience of the theory presented in Ref. 22, which gives a possible mechanism for some of the decrease in performance of cells containing djurleite compared to normal chalcocite cells.

First, an expression is derived for the spectral response of the cell, assuming absorption only in the cuprous sulfide; then it is shown that this expression together with absorption data for chalcocite provide a reasonable prediction of the chalcocite cell's spectral response characteristic. However, when applied to the djurleite cell, without changing any of the parameters used to fit the chalcocite data; the predicted response is too great (see Fig. 2.2). It is then proposed that the difference between the response predicted and that observed could be due to the effects of lattice misfit-accommodation dislocations. Applying expressions derived in the literature to the Cu_xS-CdS junction, and using data for carrier capture cross-sections found in dislocated Ge, it is demonstrated that it is reasonable for the ~0.5% lattice mismatch between chalcocite and djurleite to give rise to a more effective recombination plane than the ~4.5% mismatch between chalcocite and CdS. This paradoxical result is due to the increase in transmission probability of carriers traversing a plane of recombination centers when there is a driving electric field; the chalcocite-CdS dislocation array is argued to be in the depletion layer electric field, while the djurleite-chalcocite array will be in an essentially field-free region. Further, it is argued that the

djurleite-chalcocite array will be inhibited from climbing into the depletion layer by the repulsive interaction between the two arrays.

A necessary assumption in this argument is that the increased interfacial energy associated with the greater lattice mismatch between djurleite and CdS (compared to that between chalcocite and CdS) will inhibit the nucleation of djurleite during the dipping process in which the junction is formed, so that initially the entire junction area is a chalcocite-CdS heterojunction. This view is supported by the result of the present work which indicates that a $Cd_{1-y}Zn_yS/Cu_xS$ cell contained a mixture of djurleite and chalcocite while a CdS/Cu_xS cell formed under identical dipping conditions contained only chalcocite.

REFERENCES

1. F. Daniels, Direct Use of the Sun's Energy (Yale University Press, New York, 1974).

2. P. F. Lindquist, Physical and Photoelectronic Properties of Cuprous Sulfide-Cadmium Sulfide Heterojunctions (Ph. D. thesis), Stanford University, 1970. Many results of the above thesis were published in the following: P. F. Lindquist and R. H. Bube, 8th IEEE Photovoltäic Specialists' Conf. (Seattle, Washington, 1970). P. F. Lindquist and R. H. Bube, J. Electrochem. Soc. 119, 936 (1972). P. F. Lindquist and R. H. Bube, J. Appl. Phys. 43, 2839 (1972).

3. D. C. Reynolds, G. Leies, L. L. Antes and R. E. Marburger, Phys. Rev. 96, 533 (1954).

4. R. Williams and R. Bube, J. Appl. Phys. 31, 968 (1960).

5. H. G. Grimmeiss and R. Memming, J. Appl. Phys. 33, 2217 (1962).

6. D. A. Cusano, Sol. St. Electron. 6, 217 (1963).

7. N. DucCuong and J. Blair, J. Appl. Phys. 37, 1660 (1966).

8. A. E. Potter, Jr. and R. L. Schalla, NASA TN D-3849 (1967).

9. M. Aven and C. A. Mead, Appl. Phys. Lett. 7, 8 (1965).

10. V. A. Williams, J. Electrochem. Soc. 113, 234 (1966).

11. G. H. Blount, M. W. Fisher, R. G. Morrison and R. H. Bube, J. Electrochem. Soc. 113, 690 (1966).

12. R. G. Kaufman and P. Dowbor, J. Appl. Phys. 45, 4487 (1974). This work also discusses a possible mechanism for the formation of ohmic contacts to cadmium and zinc chalcogenides.

13. P. Cherin, E. L. Linde and E. A. Davis, J. Electrochem. Soc. 117, 233 (1970).

14. E. A. David and E. L. Lind, J. Phys. Chem. Sol. 29, 79 (1968).

15. G. H. Blount, A. C. Sanderson and R. H. Bube, J. Appl. Phys. 38, 4409 (1967).

16. G. Shachar, Y. Brada and I. T. Steinberger, J. Appl. Phys. 41, 4938 (1970).

17. J. Benoit, P. Benalloul and R. David, Thin Sol. Films 8, 123 (1971).

18. A. N. Georgobiani and V. I. Steblin, phys. stat. sol. 21, K45 (1967).

19. W. Palz, J. Besson, T. N. Duy and J. Vedel, Review of CdS Solar Cell Activities, in Conf. Record of the 10th IEEE Photovoltäic Specialists Conf., 1973, Palo Alto (California).

20. K. W. Böer, L. Burton, H. Hadley, J. Phillips, A. Rothward, G. Storti and H. Windawi, International Solar Energy Society, 1975 International Solar Energy Congress and Exposition, July 28-Aug. 1, 1975, Los Angeles, California.

21. S. M. Sze, Physics of Semiconductor Devices (John Wiley & Sons, Inc., New York, 1969), p. 104ff. Note: There is a common ambiguity in the literature regarding the vacuum level (see Fig. 2.1). If one defines the vacuum level to be that energy of an electron isolated at infinity, it will be a constant value everywhere, as shown in Fig. 2.1. However, this definition runs into trouble when one talks about "semi-infinite" slabs of material, since there is no way to isolate an electron at infinity. Therefore, the diagram in Fig. 2.1 is interpreted as applying to large, but finite, pieces of semiconductor.

22. T. Peterson and J. Washburn, phys. stat. sol. (a) 22, 721 (1974).

23. W. Palz, J. Besson, T. Nguyen Duy and J. Vedel, 9th IEEE Photovoltäic Specialists Conference (May 1972).

24. T. S. TeVelde, Sol. St. Electron. 16, 1305 (1973).

25. B. J. Mulder, phys. stat. sol. (a) 13, 79 (1972).

26. W. D. Gill, Photovoltäic Properties of Cu_2S-CdS Heterojunctions (Ph. D. thesis), Stanford University, 1969. Some results of the above thesis were published in the following: W. D. Gill and R. H. Bube, J. Appl. Phys. 41, 1694 (1970). W. D. Gill and R. H. Bube, J. Appl. Phys. 41, 3731 (1970).

27. G. H. Hewig, Herstellung, Untersuchungsmethoden und Theoretische Behandlung von Cu_xS-CdS-Dünnschicht-Solarzellen (Dr.-Ing. thesis), Universität Stuttgart, 1974 (in German). Parts appear in English in Chapter 2.6. Proceedings: International Conference on Photovoltäic Power Generation, Hamburg (Sept. 25-27, 1974).

28. L. I. Schiff, Quantum Mechanics (McGraw-Hill, New York, 1968), p. 101ff.

29. A. L. Fahrenbruch and R. H. Bube, Journal of Applied Physics 45, 1264 (1974).

30. B. J. Mulder, phys. stat. sol. (a) 18, 633 (1973).

31. T. M. Peterson, LBL Report, LBL-3751, Lawrence Berkeley Laboratory.

32. Mr. Richard Lindberg did the microprobe work reported here.

33. J. W. Colby, Bell Telephone Laboratories, Allentown, PA.

34. A. L. Fahrenbruch, Heat Treatment Effects in Cu_2S-CdS Heterojunction Photovoltäic Cells (Ph. D. thesis), Stanford University, 1973. See also, Ref. 29 and the following: A. L. Fahrenbruch and R. H. Bube, 9th IEEE Photovoltäic Specialists' Conf. (Silver Spring, MD, 1972).

A. L. Fahrenbruch and R. H. Bube, 10th IEEE Photovoltaic Specialists' Conference (Palo Alto, CA, 1973).

FIGURE CAPTIONS

Fig. 2.1. (a) Band diagrams of two isolated, finite semiconductors with no surface charge accumulation/depletion and differing gaps E_{gi}, electron affinities χ_i, and types. (b) The same two semiconductors after establishment of intimate contact. Note increase in electron affinity $\Delta\chi$; the magnitude of which depends on the sizes of the semiconductors, the barrier voltage, etc.; but the existence of which can be argued from general thermodynamic grounds (see note to Ref. 21).

Fig. 2.2. Comparison of spectral response of Cu_xS/CdS cell calculated using cuprous sulfide absorption data of Mulder (Ref. 25) with that measured in thin film cells in Palz, et al. (Ref. 23). From Ref. 22.

Fig. 2.3. Transmission of monoenergetic electrons at a simple triangular barrier vs electron energy.

Fig. 2.4. Integrated transmission of Maxwell-Boltzmann distribution of electrons (kT = 0.025 eV) at a simple triangular barrier vs total depletion layer thickness W.

Fig. 2.5. Integrated transmission of a Maxwell-Boltzmann electron distribution at abrupt positive and negative steps in otherwise constant potentials vs step height.

Fig. 2.6. Integrated transmission of a Maxwell-Boltzmann electron distribution at a negative step potential vs step width.

Fig. 2.7. As Fig. 2.3, but using potential shown in Fig. 2.9.

Fig. 2.8. As Fig. 2.4, but using potential shown in Fig. 2.9.

Fig. 2.9. Potential used for calculations of Figs. 2.7 and 2.8:

$$V(x) = \begin{cases} 0 & , x < -x_1 \\ -V_{b1}(1 + x/x_1)^2 & , -x_1 \leq x \leq 0 \\ \Delta(x/\delta) - V_{b1} & , 0 \leq x < \delta \\ V_{b2}[1 - (x - \delta)/W]^2 - V_D & , \delta \leq x < x_2 \\ -V_D & , x_2 \leq x \end{cases}$$

where $V_{b1} = \dfrac{V_D}{1 + N_1/N_2}$, $V_{b2} = V_D + \Delta - V_{b1}$

$x_1 = W(N_2/N_1)$, $x_2 = W + \delta$.

Fig. 2.10. Rigid-band model of cuprous sulfides showing band gaps and fermi levels of chalcocite (Cu_2S) and djurleite ($Cu_{1.95}S$).

Fig. 3.1. Schematic diagram of I-V measurement apparatus.

Fig. 3.2. Schematic diagram of spectral response measurement apparatus.

Fig. 4.1. Electron microprobe scan perpendicular to striations in optical properties of $Cd_{0.75}Zn_{0.25}S$ crystal.

Fig. 4.2. (a) I-V characteristic of Ag/ZnS Schottky barrier on ZnS sample allowed to cool to 400°C from 950°C in about 2.5 hr after the doping firing. (b) As above, but ZnS sample (in quartz ampoule) removed from 950°C furnace to ambient. Scales in (a) and (b): Horizontal, 1 V/div; vertical, 10 μA/div. Upper trace is with focused microscope lamplight; lower trace, with room lights only. (c) Same sample as (a), but in total darkness. Scales: Horizontal, 10 V/div; Vertical, 100 μA/div.

Fig. 4.3. (a) I-V characteristic of cell #1Z9-26 under microscope lamp. Scales: Horizontal, 0.5 V/div; Vertical, 2 μA/div. (b) I-V characteristic of "aged" cell #1Z4-12 in sunlight (2:30 PM, PDT, 5/30/74). Scales: Horizontal, 0.5 V/div; Vertical, 20 μA/div. (c) I-V characteristic of cell #1Z4-12 in sunlight (2 PM, PDT, 4/12/74). Scales: Horizontal, 0.5 V/div; Vertical, 50 μA/div (0.35 mA/cm^2-div).

Fig. 4.4. I-V characteristic of cell #C8-16 in sunlight (1:50 PM, PDT, 8/20/75) and with filters--see note. Vertical scale: 0.5 mA/div (1.7 mA/cm^2-div). (b) As in (a), but with focused microscope lamplight. Vertical scale: 2 mA/div.

Fig. 4.5. (a) I-V characteristic of cell #M8-16 in sunlight (1:45 PM, PDT, 8/20/75) and with filters--see note. Vertical scale: 0.1 mA/div (1 mA/cm^2-div). Note to 4.6 and 4.7: The horizontal scales are all 0.2 volt/division; and the traces in order to increasing I_{sc} are (1) dark, (2) $\lambda > 700$ nm, (3) $\lambda > 630$ nm and (4) no filter.

Fig. 4.6. Short-circuit current of Cu_xS/ZnS cell vs wavelength of constant intensity incident light.

Fig. 4.7. Short-circuit current of CdS/Cu_xS cell vs wavelength of constant intensity incident light.

Fig. 4.8. Short-circuit current of $Cd_{0.75}Zn_{0.25}S/Cu_xS$ cell vs wavelength of constant intensity incident light.

Fig. 5.1. Band diagram of heterojunction of ZnS with chalcocite and djurleite.

Fig. A.1. Fortran subprogram which calculates electron transmission probabilities as described in Appendix A.

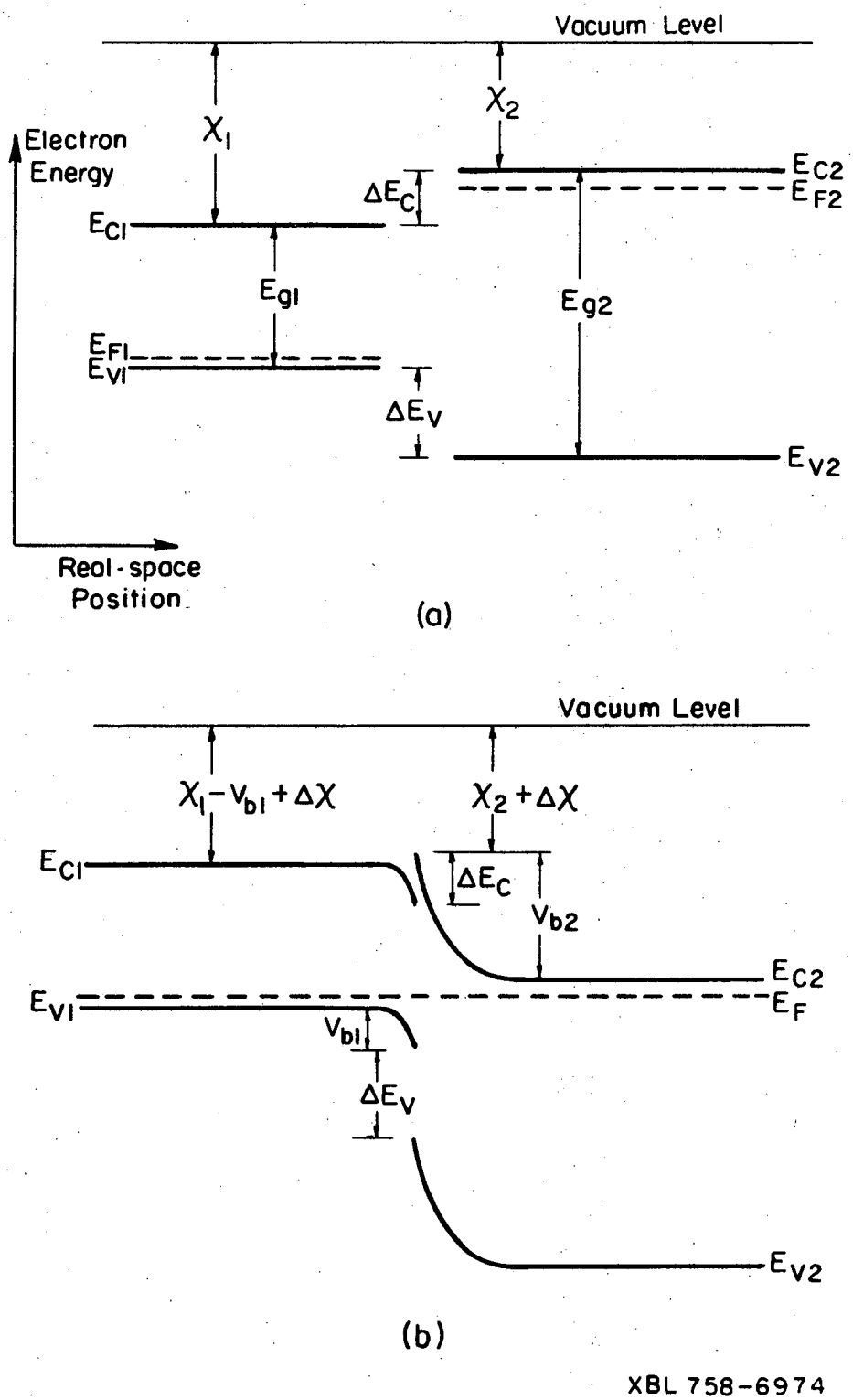
Vacuum Level
χ_1
χ_2
Electron Energy
E_{C2}
E_{F2}
ΔE_C
E_{C1}
E_{g1}
E_{g2}
E_{F1}
E_{V1}
ΔE_V
E_{V2}
Real-space Position
(a)
Vacuum Level
$\chi_1 - V_{b1} + \Delta\chi$
$\chi_2 + \Delta\chi$
E_{C1}
ΔE_C
V_{b2}
E_{C2}
E_{V1}
E_F
V_{b1}
ΔE_V
E_{V2}
(b)
XBL 758-6974

Fig. 2.1

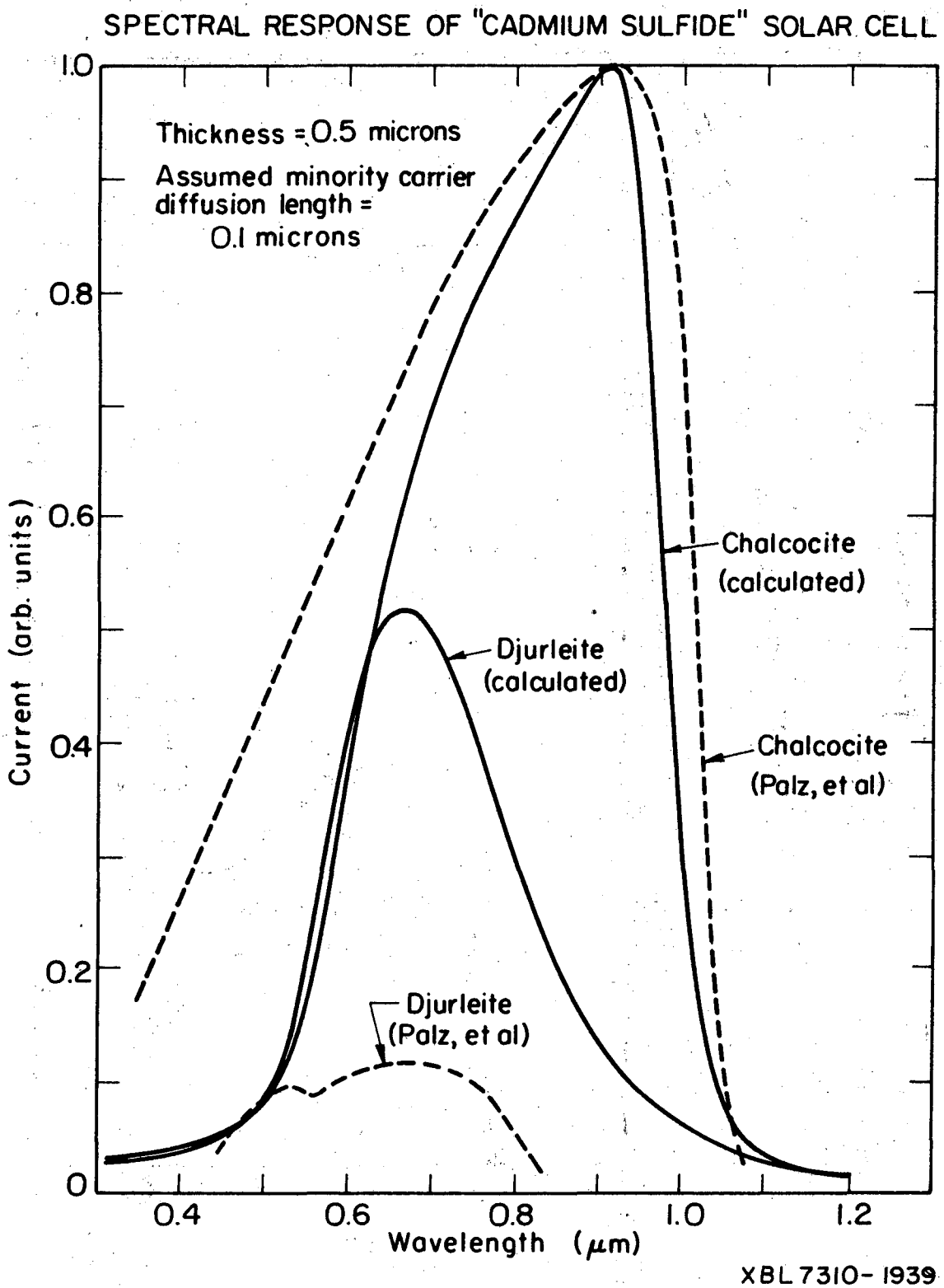

Fig. 2.2

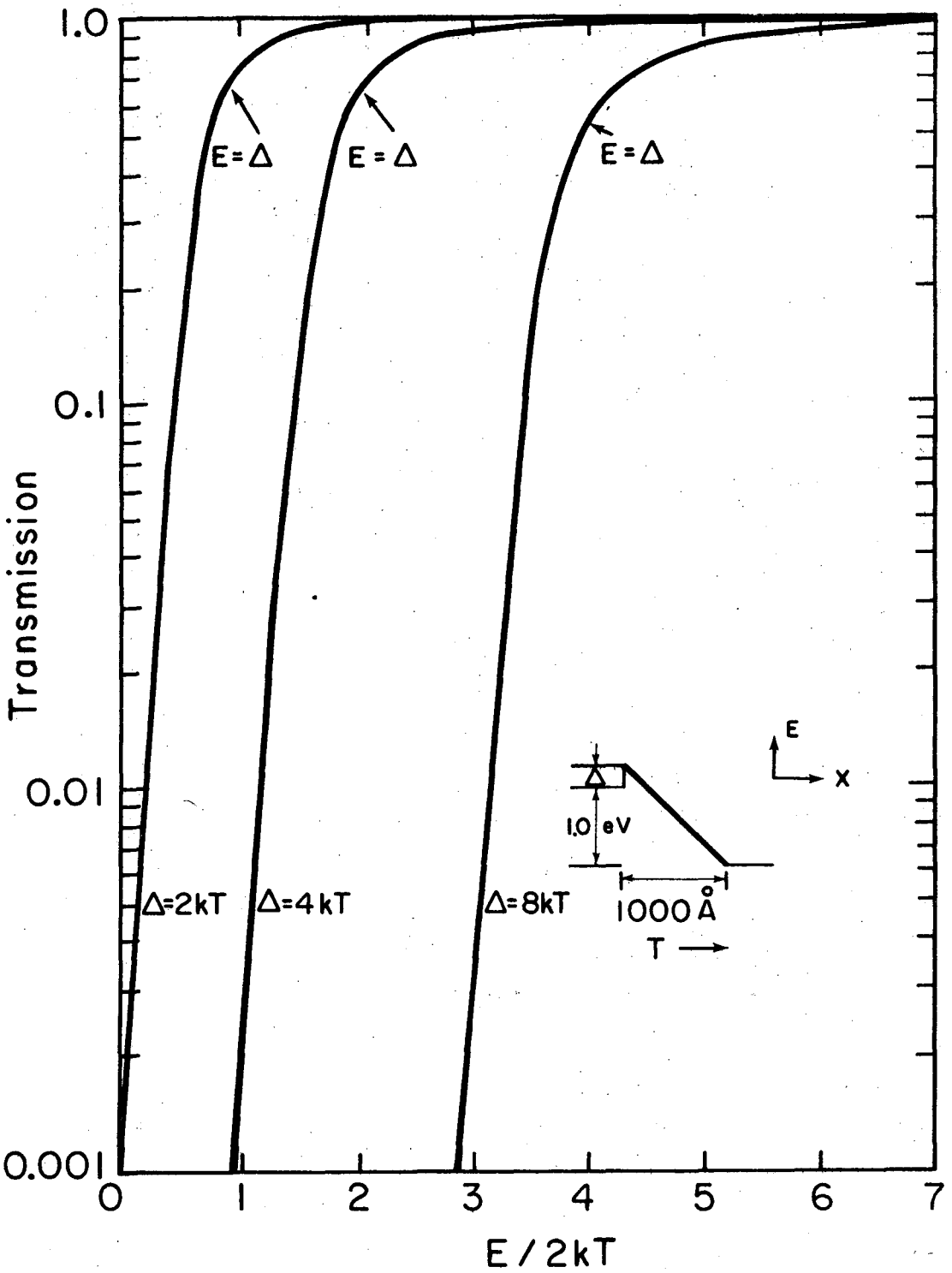
1.0
0.1
0.01
0.001
Transmission
E = Δ
E = Δ
E = Δ
Δ=2kT
Δ=4kT
Δ=8kT
E
X
1.0 eV
1000 Å
T
0
1
2
3
4
5
6
7
E / 2kT
XBL755-2905

Fig. 2.3

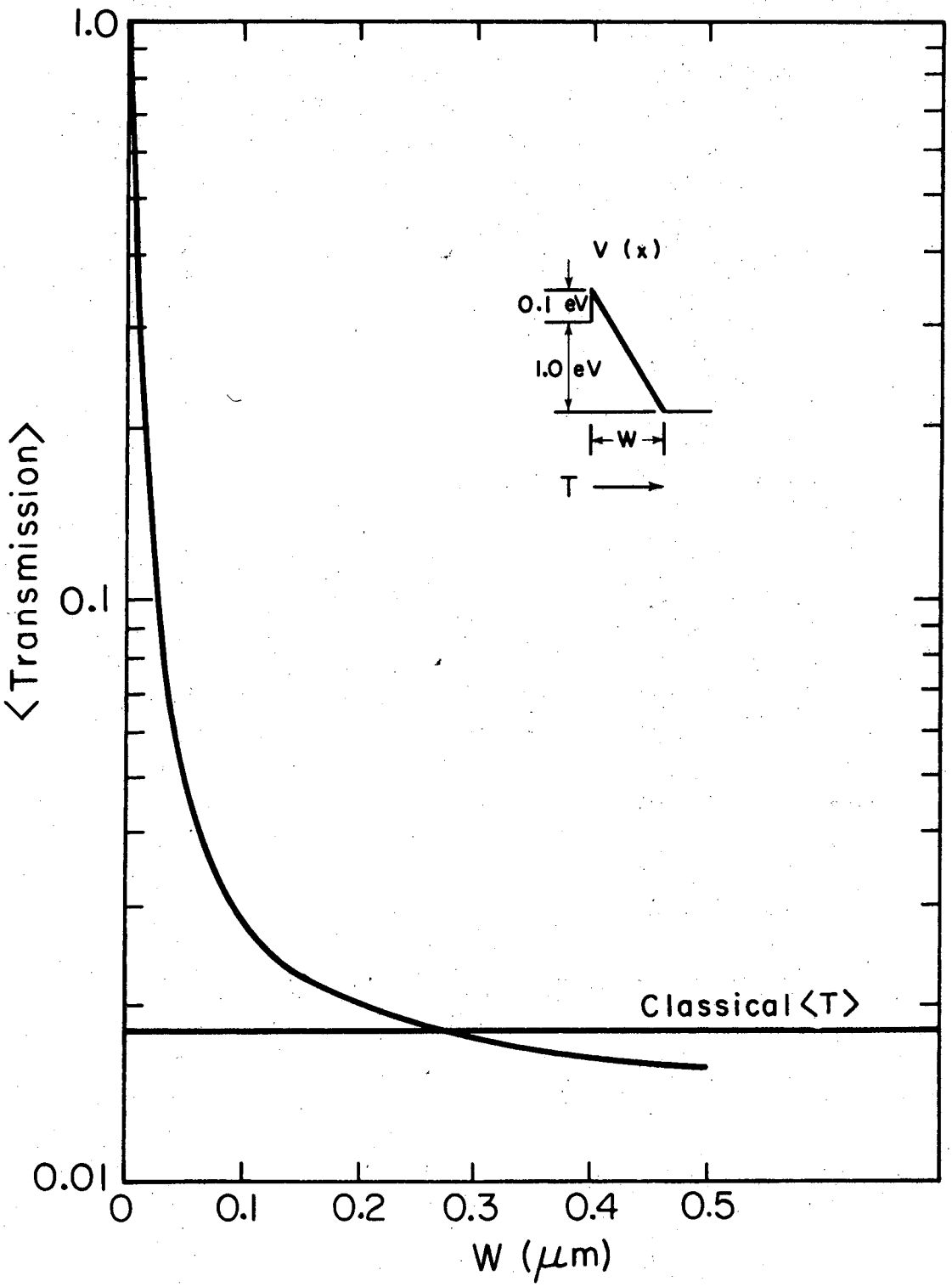

XBL755-2906

Fig. 2.4

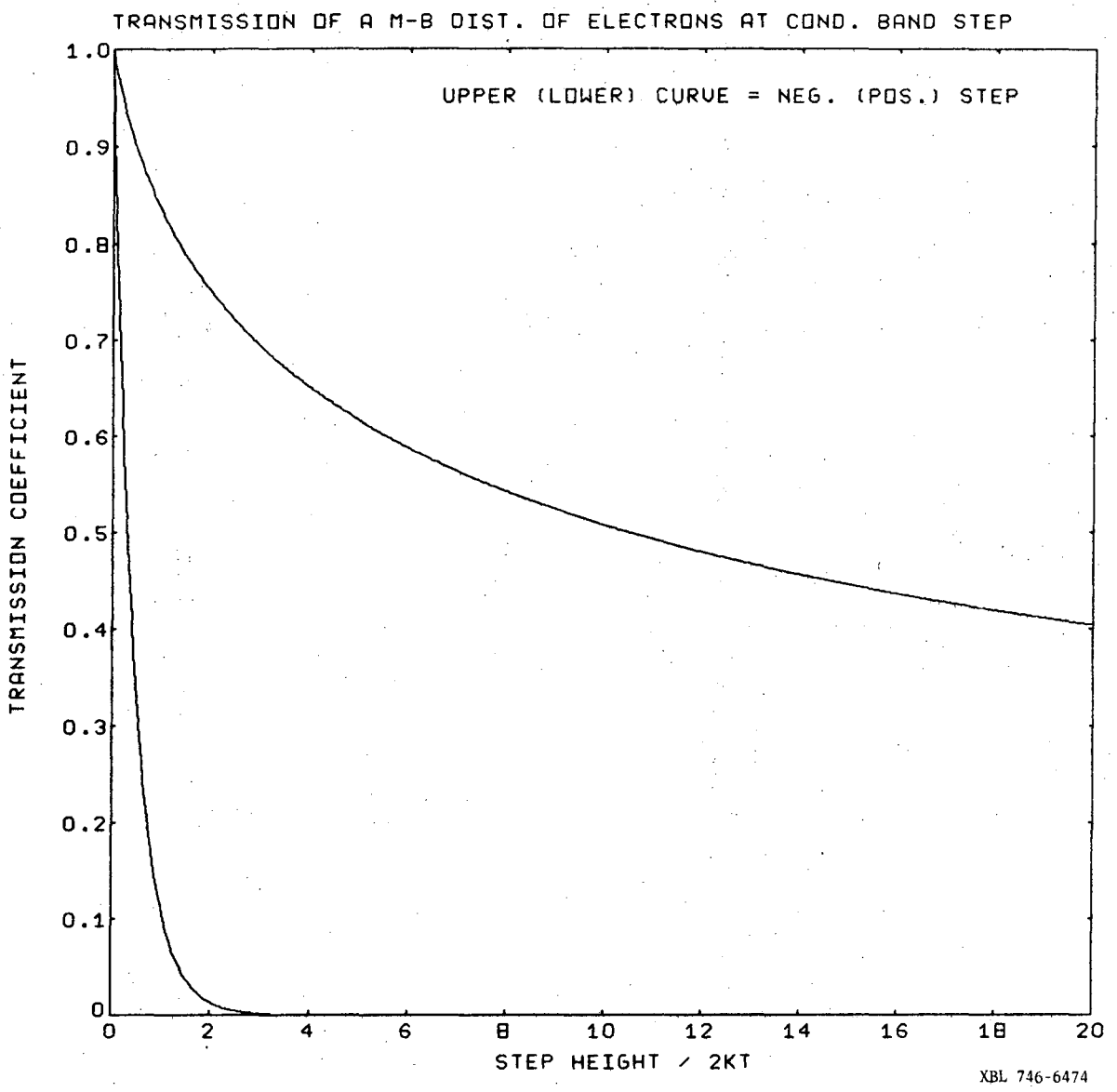
TRANSMISSION OF A M-B DIST. OF ELECTRONS AT COND. BAND STEP
UPPER (LOWER) CURVE = NEG. (POS.) STEP
TRANSMISSION COEFFICIENT
1.0
0.9
0.8
0.7
0.6
0.5
0.4
0.3
0.2
0.1
0
0
2
4
6
8
10
12
14
16
18
20
STEP HEIGHT / 2KT
XBL 746-6474

Fig. 2.5

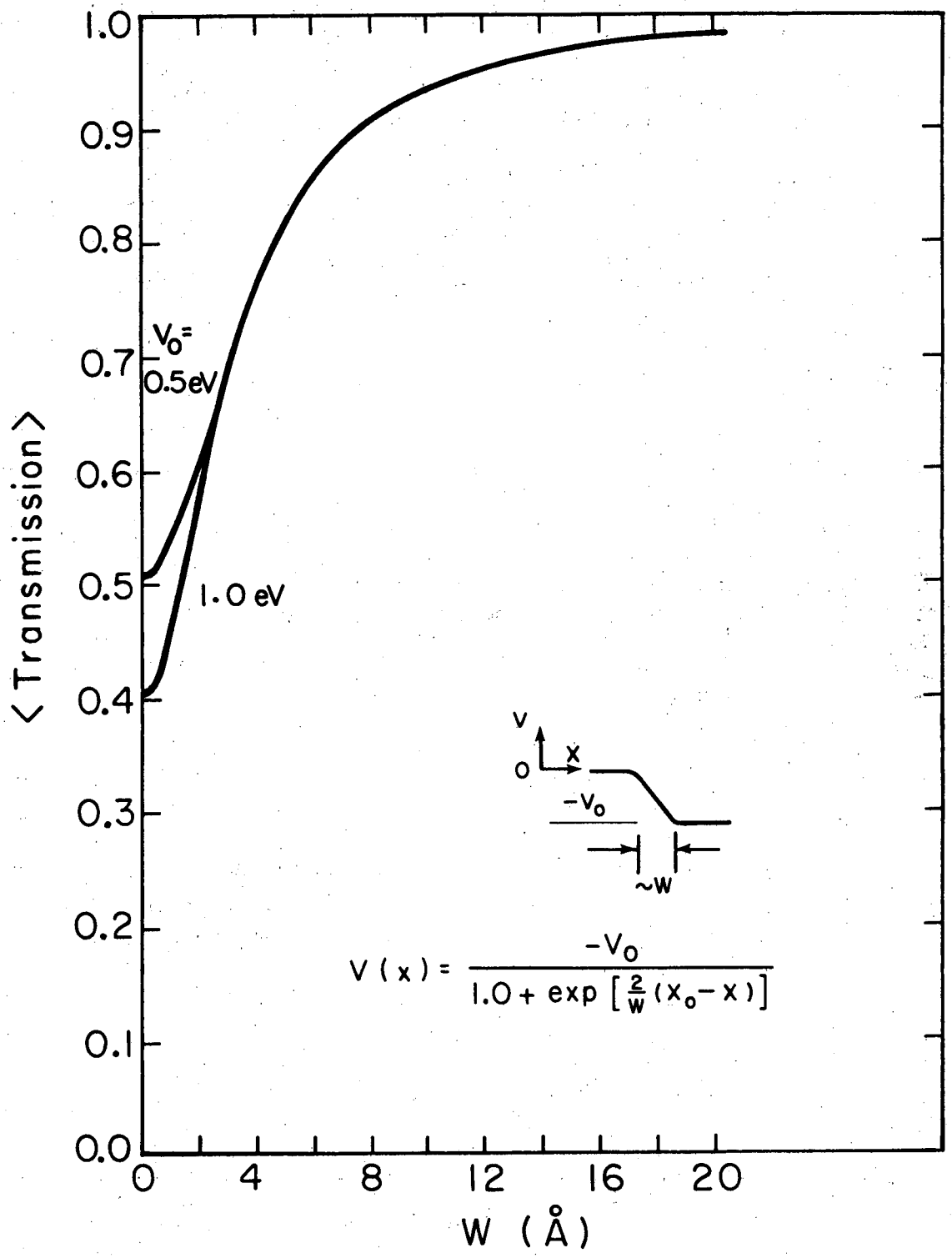

Fig. 2.6

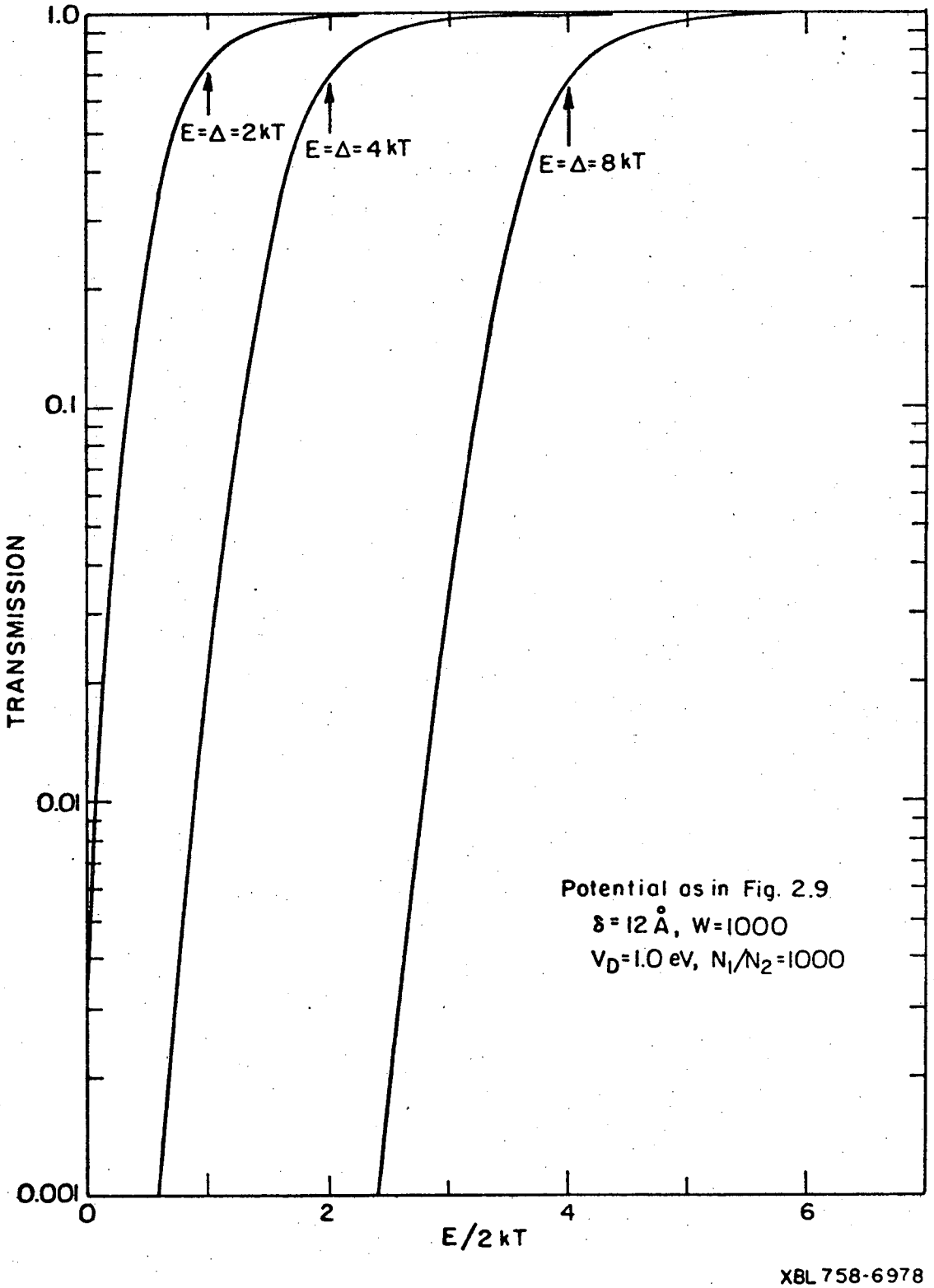
1.0
0.1
0.01
0.001
TRANSMISSION
E=Δ=2kT
E=Δ=4kT
E=Δ=8kT
Potential as in Fig. 2.9
δ = 12 Å, W=1000
V_D=1.0 eV, N_1/N_2=1000
0
2
4
6
E/2kT
XBL 758-6978

Fig. 2.7

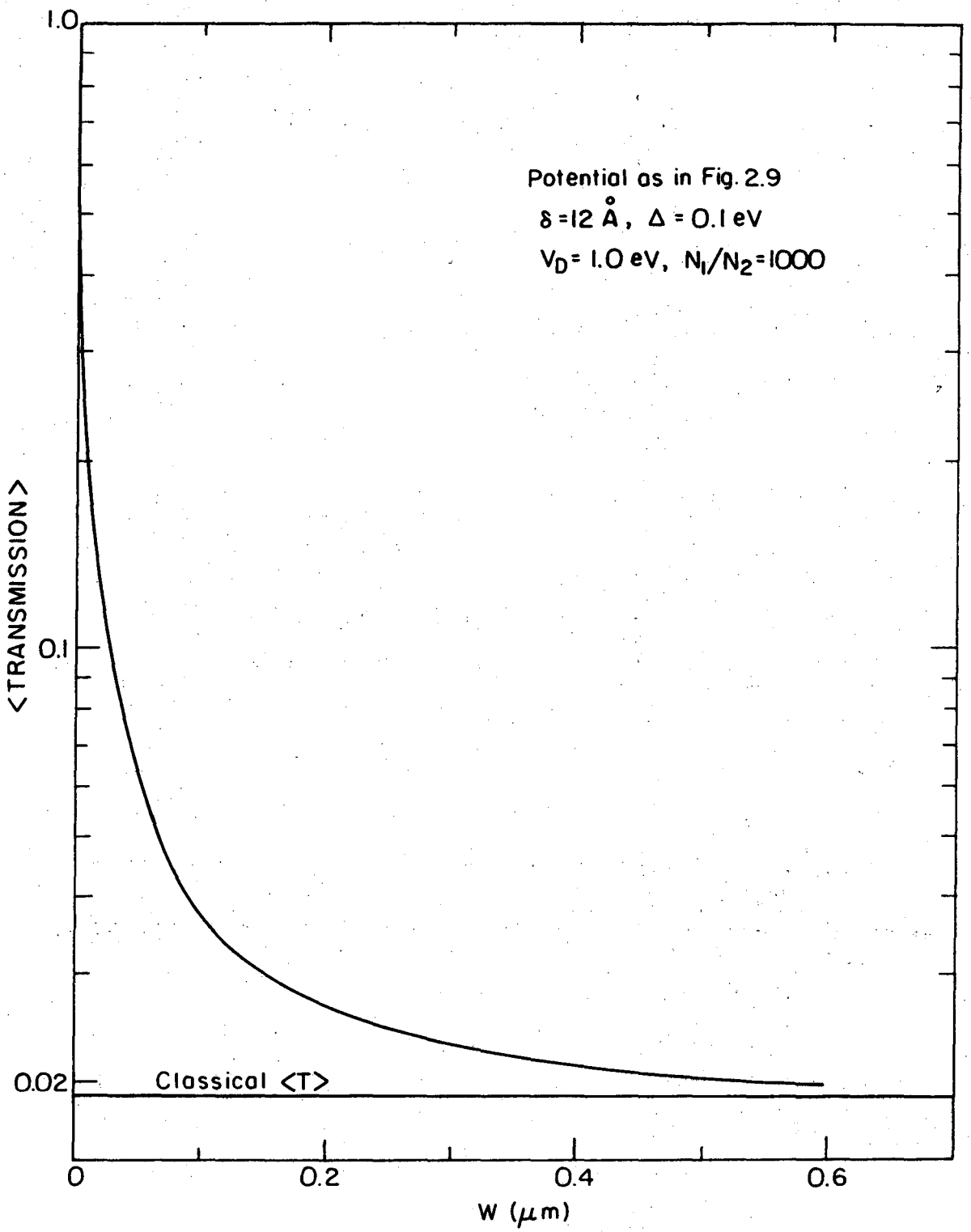

Fig. 2.8

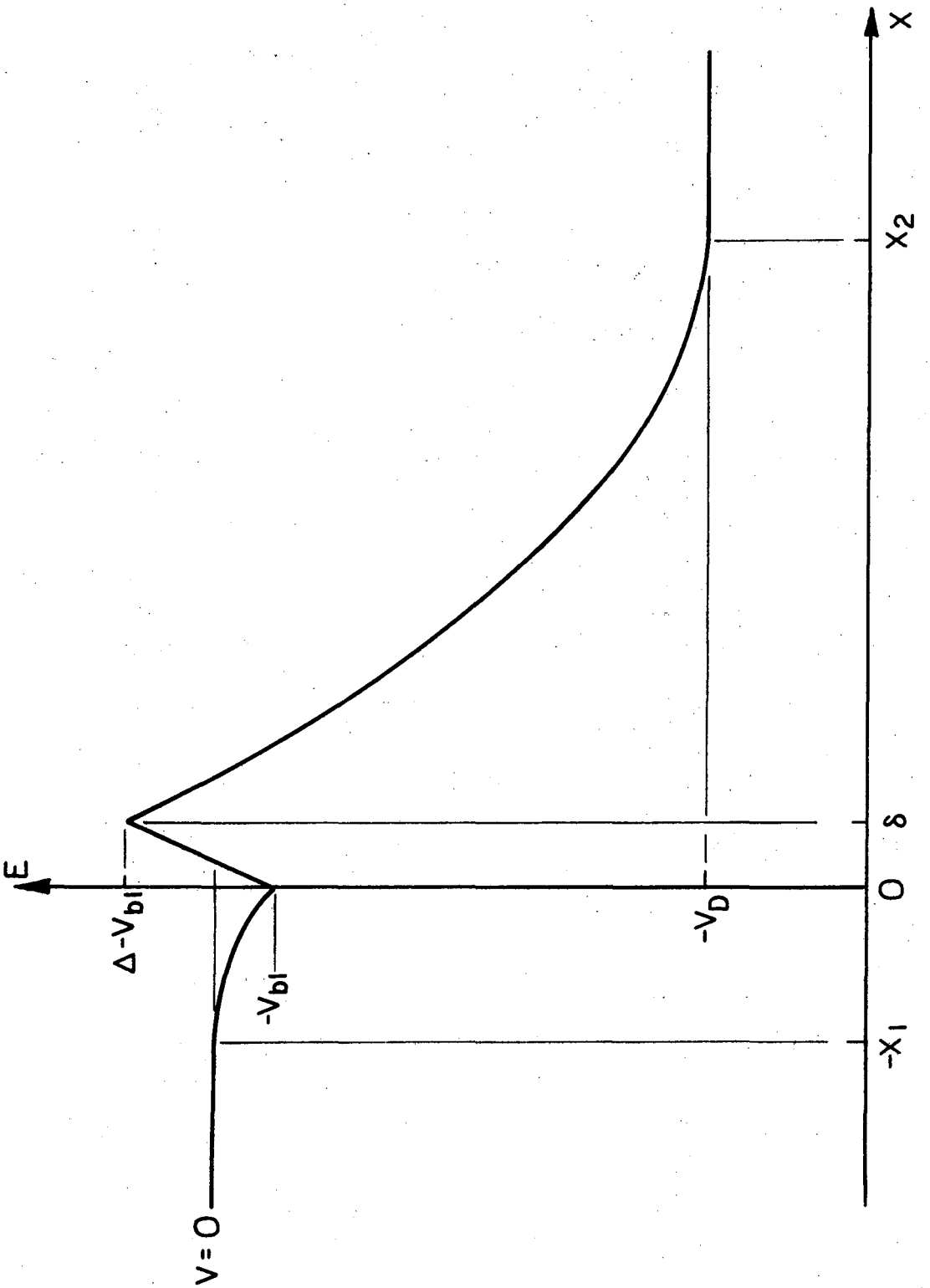

XBL 758-6977

Fig. 2.9

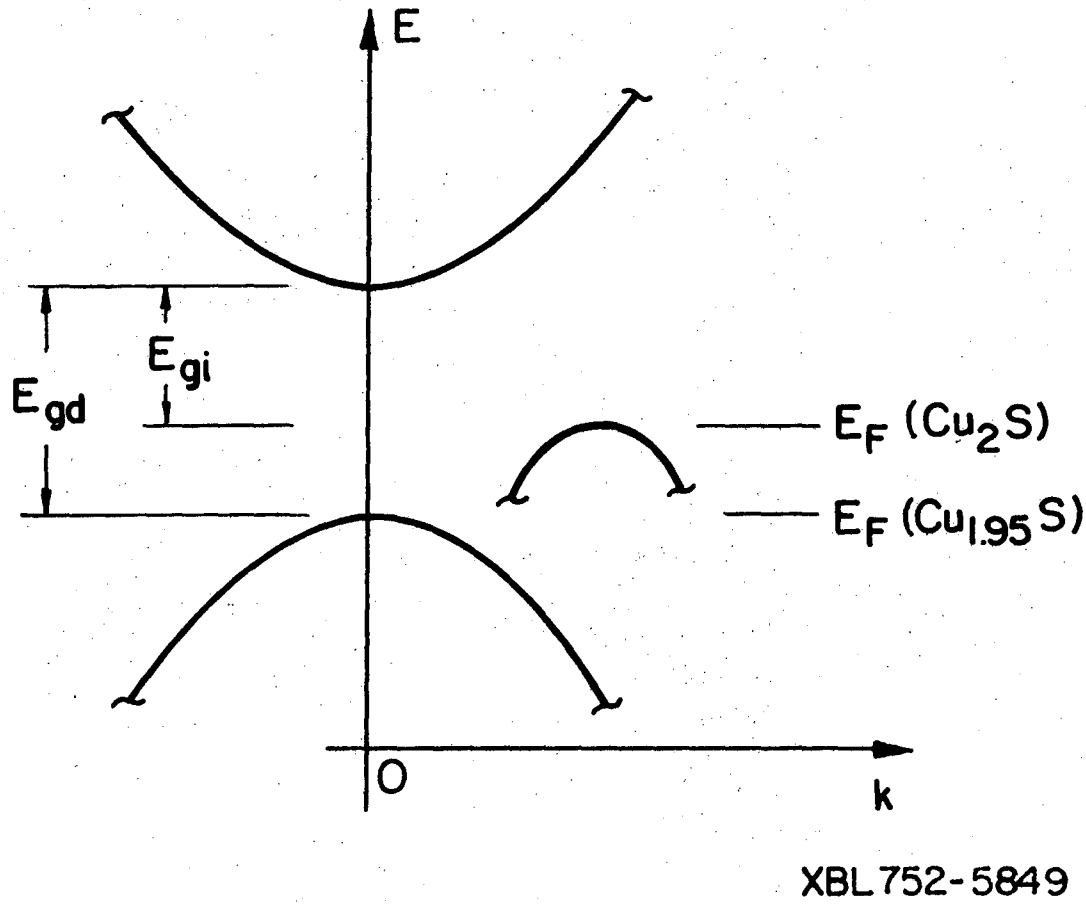

Fig. 2.10

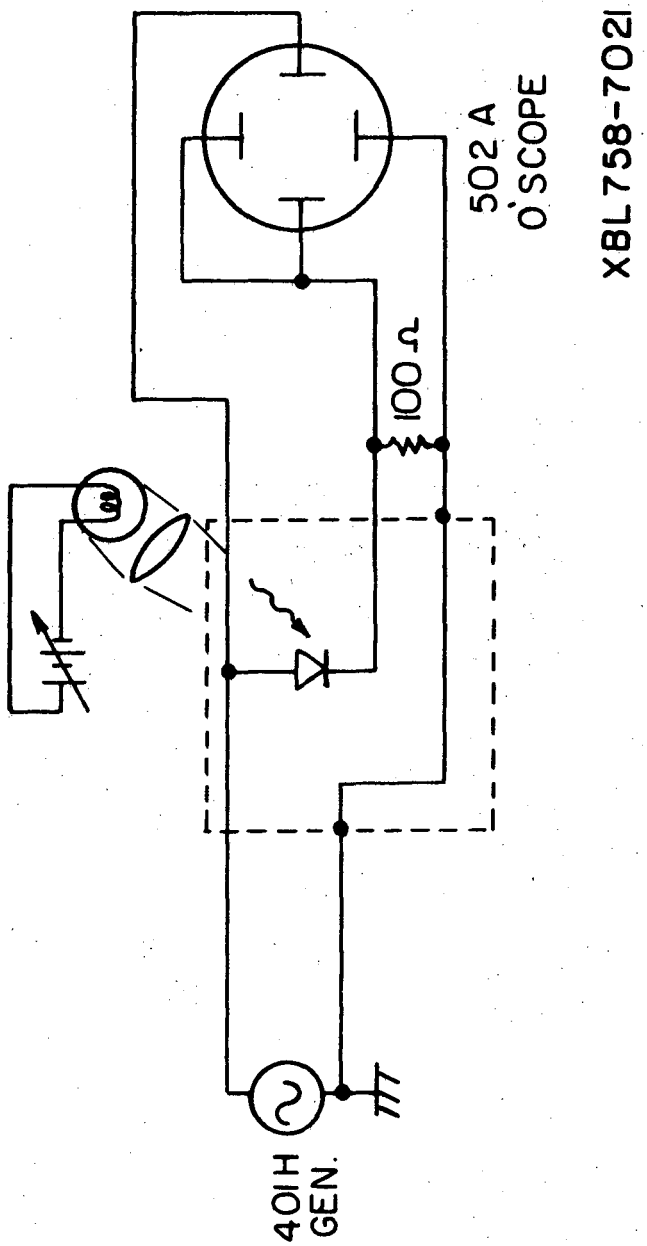

Fig. 3.1

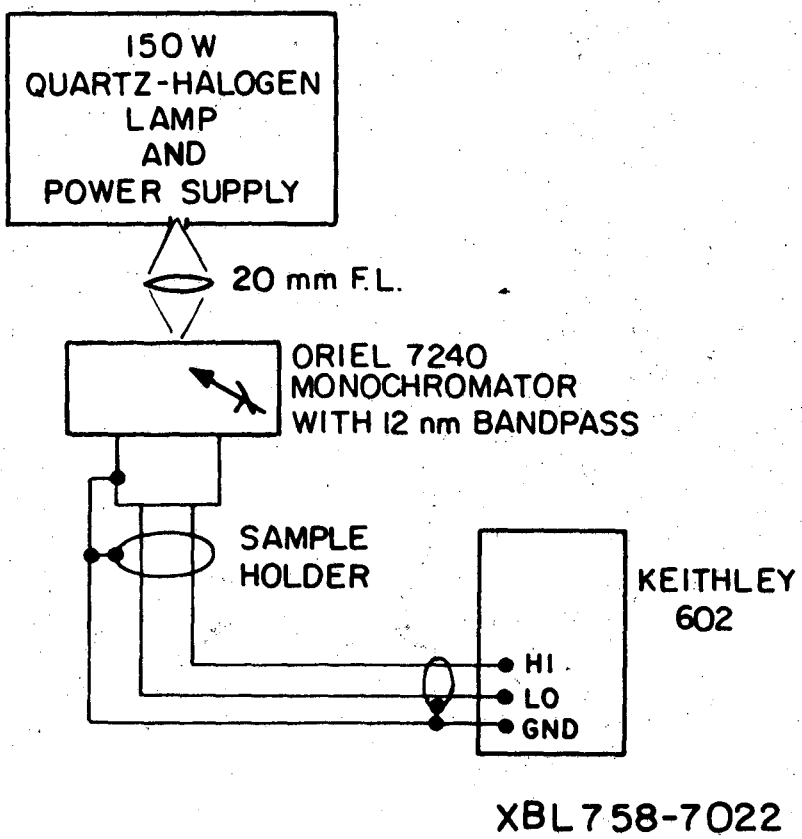

Fig. 3.2

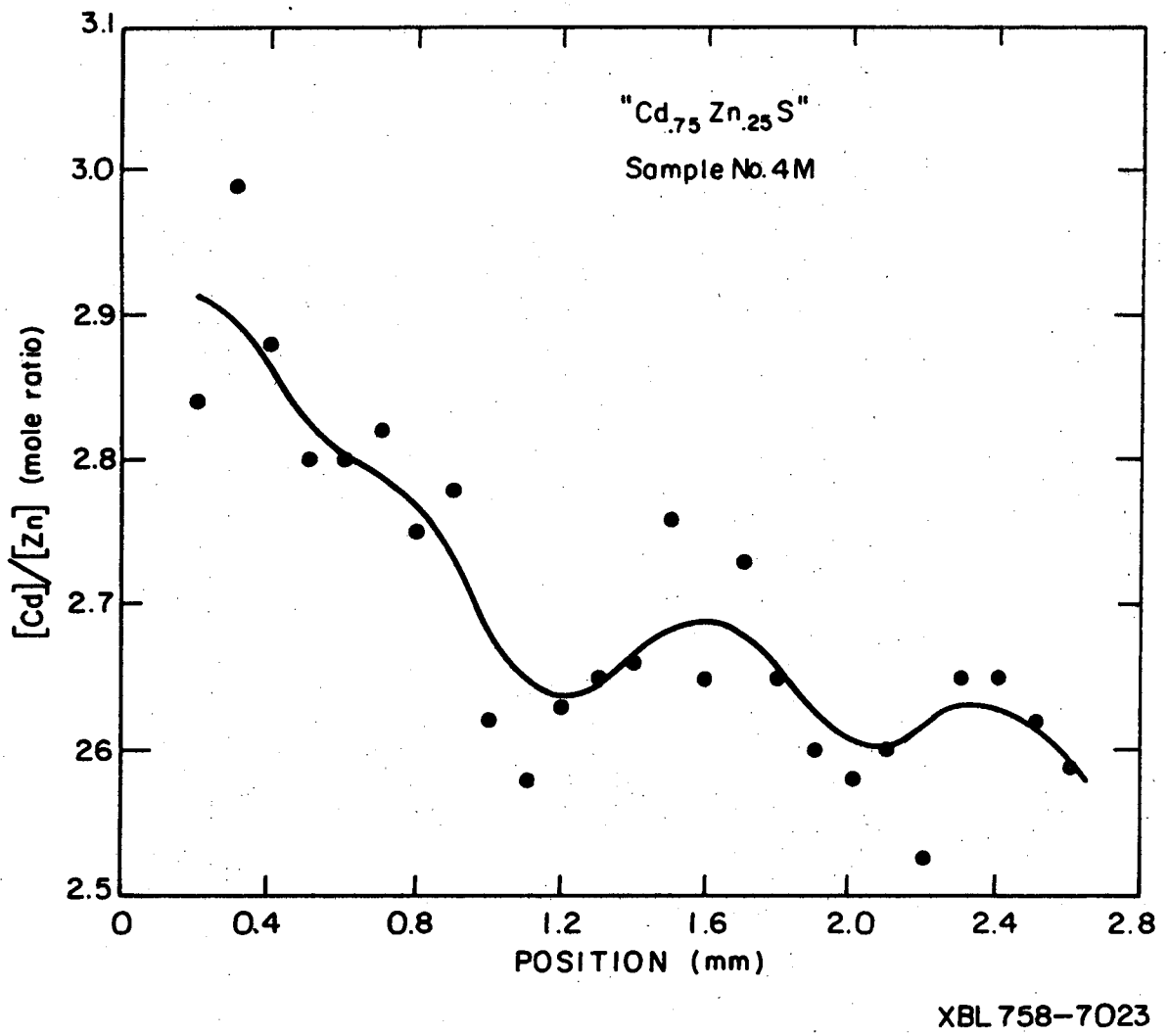
"Cd.75 Zn.25 S"
Sample No. 4M
[Cd]/[Zn] (mole ratio)
3.1
3.0
2.9
2.8
2.7
26
2.5
0
0.4
0.8
1.2
1.6
2.0
2.4
2.8
POSITION (mm)
XBL 758-7023

Fig. 4.1

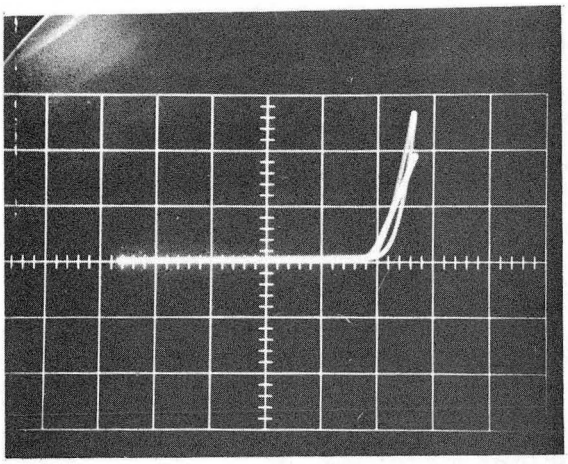

a

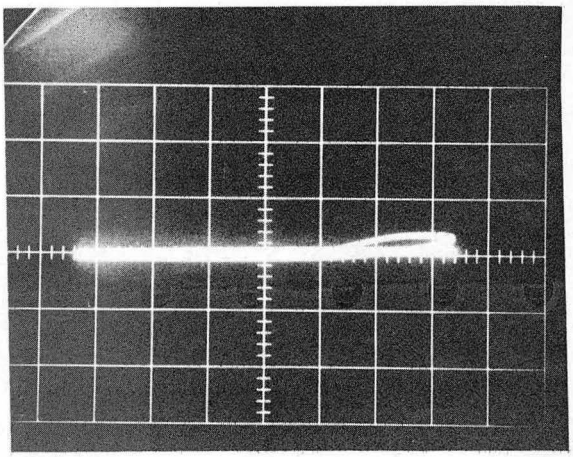

b

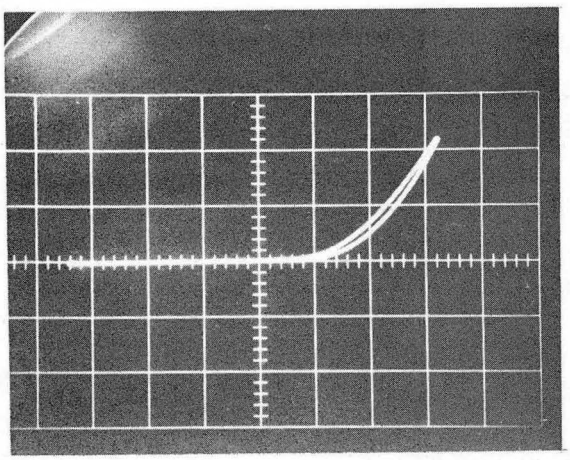

c

XBB 758-6388

Fig. 4.2

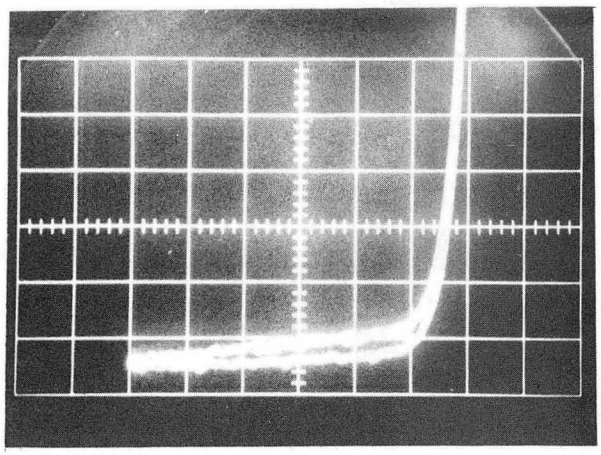

a

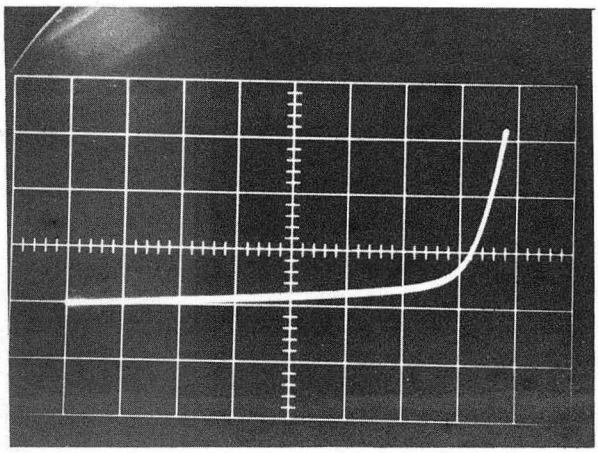

b

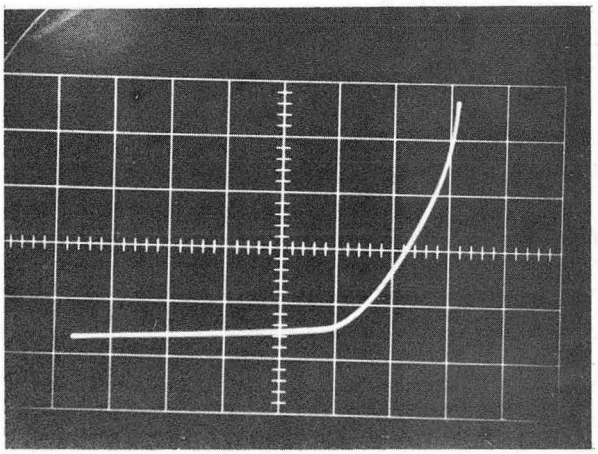

c

XBB 758-6387

Fig. 4.3

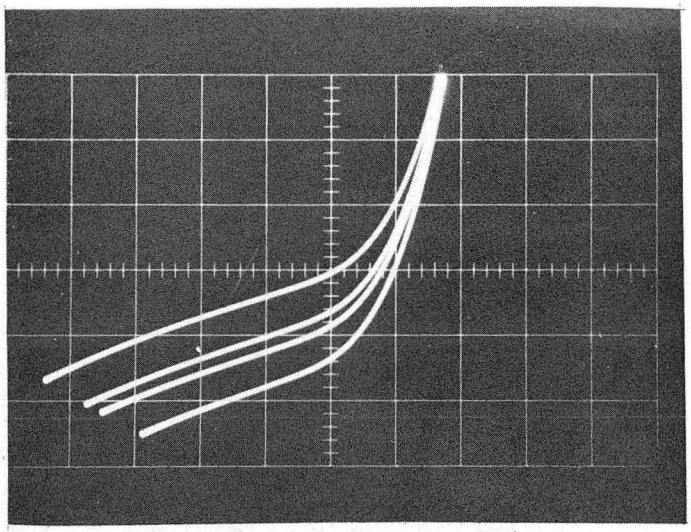

a

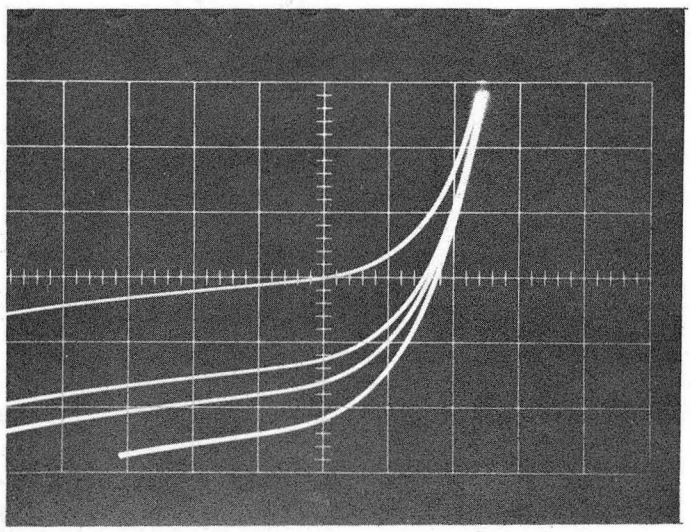

b

XBB 758-6385

Fig. 4.4

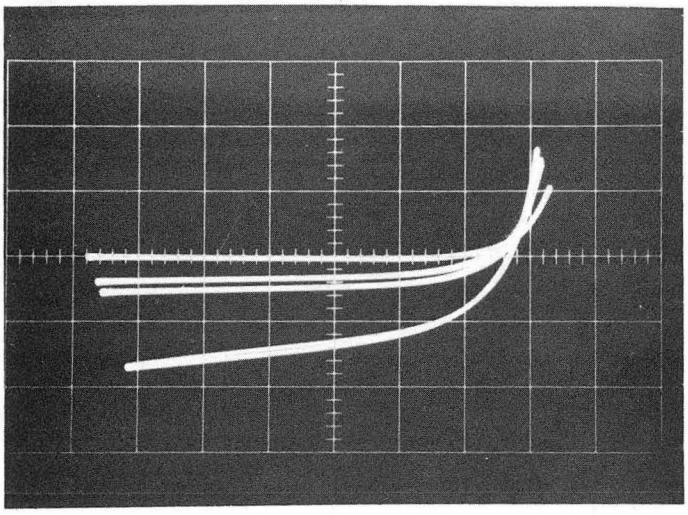

a

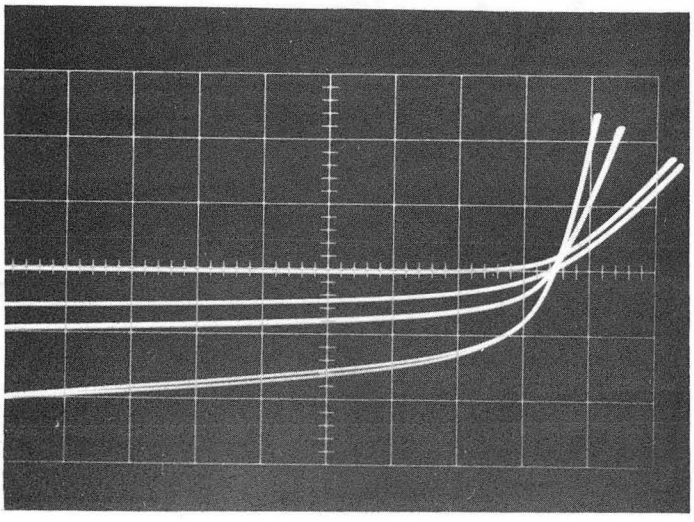

b

XBB 758-6386

Fig. 4.5

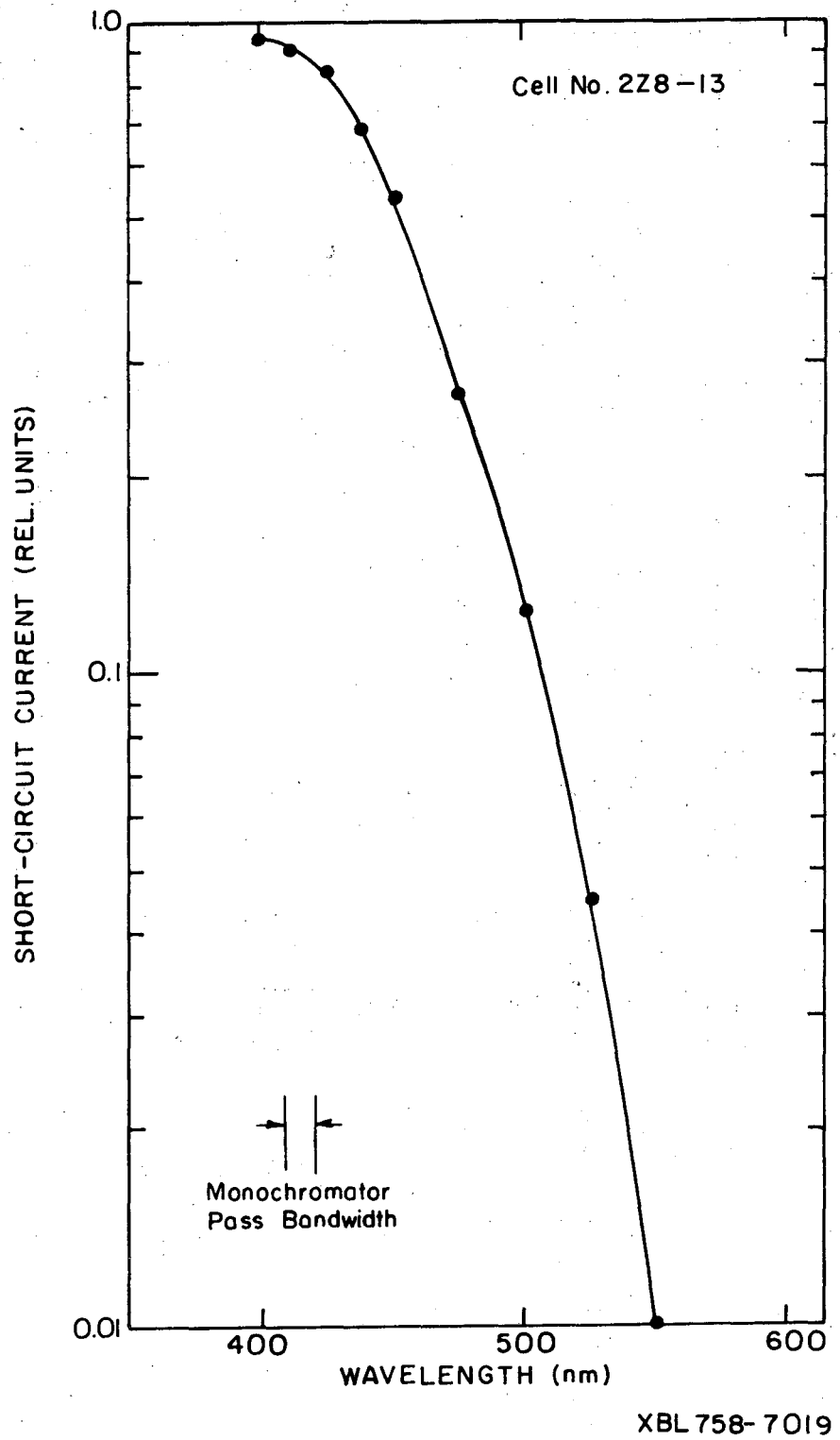

Fig. 4.6

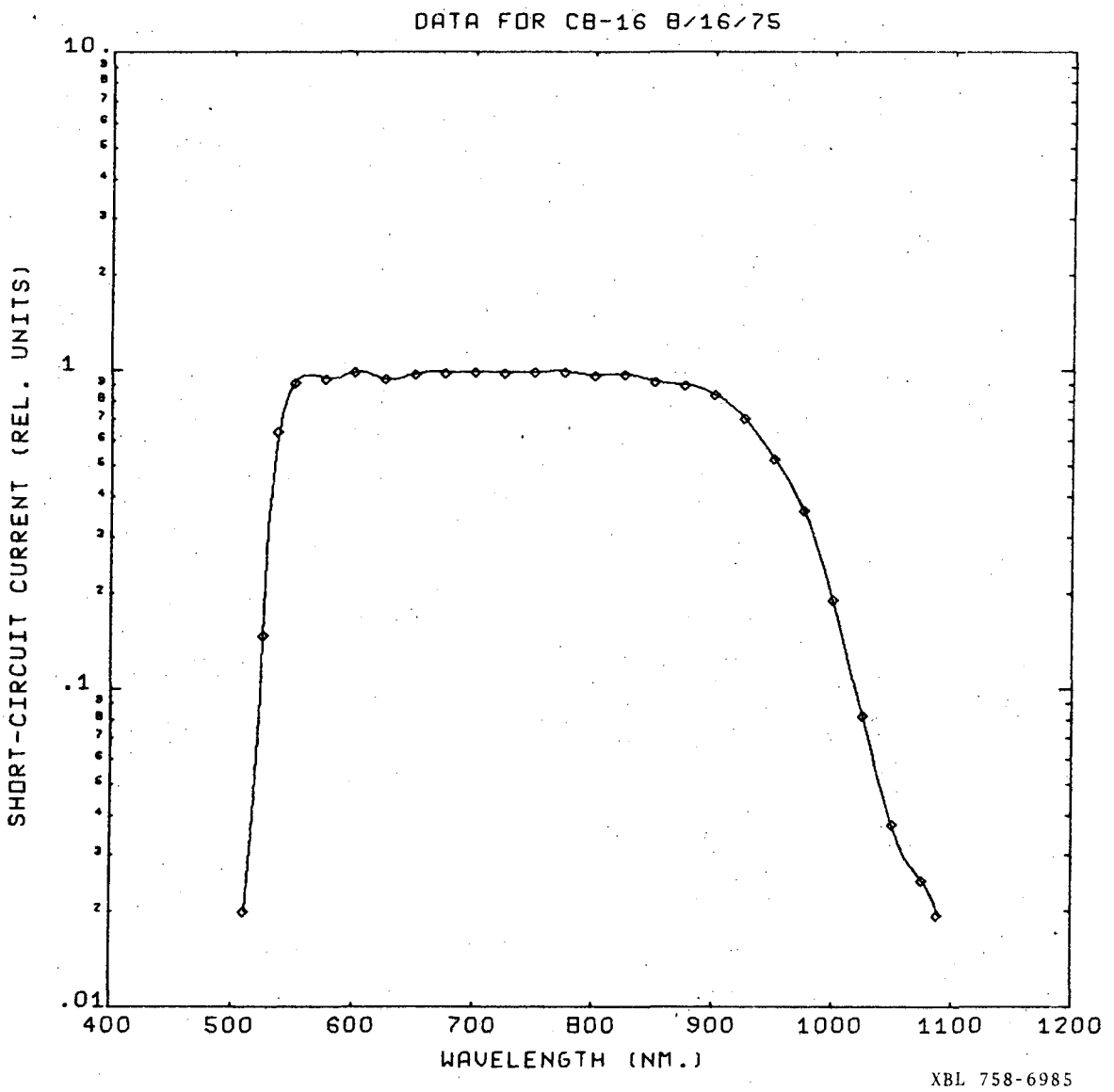
DATA FOR CB-16 8/16/75
SHORT-CIRCUIT CURRENT (REL. UNITS)
10
1
.1
.01
400
500
600
700
800
900
1000
1100
1200
WAVELENGTH (NM.)
XBL 758-6985

Fig. 4.7

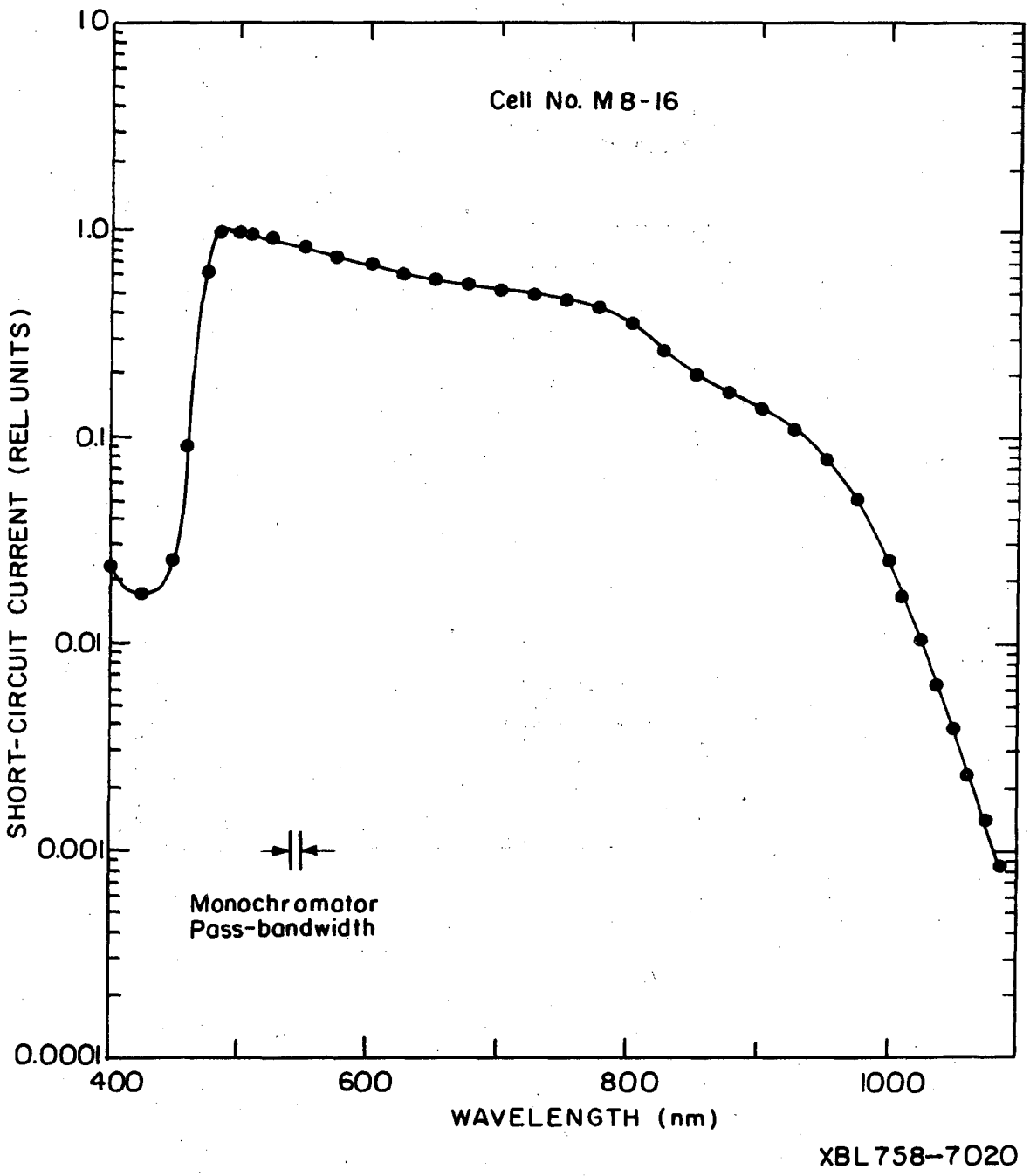

Fig. 4.8

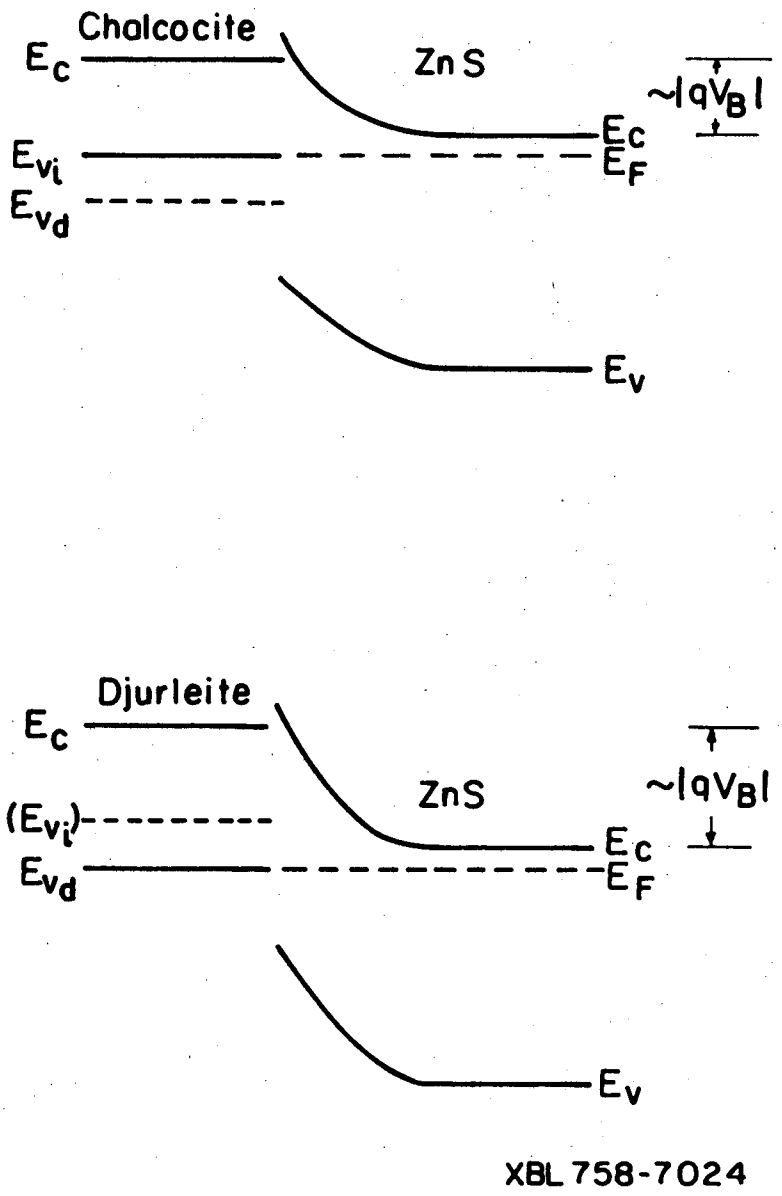
Chalcocite
E_c
ZnS
$\sim|qV_B|$
E_c
E_{v_i}
E_F
E_{v_d}
E_v
Djurleite
E_c
ZnS
$\sim|qV_B|$
(E_{v_i})
E_c
E_{v_d}
E_F
E_v
XBL 758-7024

Fig. 5.1

```
FUNCTION    T                                          CDC 7600 FTN V1.0-324H OPT=2
                    FUNCTION T(ENERGY)
                    COMPLEX   CA(4),CDELM,CDELP,CKR,CKX,CK1,CK2,CT(4),CXPN,CTO
                    COMMON XI(2001), VI(2000)
                    COMMON /RESET/ N, NMAX, XL, XU, DX, DVMAX
 5                  DATA UNITS/1.0246845/, NO/-1/
                    IF (ENERGY .LT. 1.0E-10) GO TO 20
                    E= 0.025*ENERGY
                    IF (N - NO) 2000,1000,2000
                C                                    . . . SET UP APPROX. POT. VI(XI)
10           2000   XI(2) = X = XL   $  VI(1) = V2 = V(X)
                    DO 50 N=2,NMAX
                    V1 = V2
                25  X = X + DX   $ V2 = V(X)
                    IF (X -XU) 26,26,30
15                  ABV = ABS(V2-V1)
                    IF (ABV-DVMAX)  25,25,30
                30  XI(N+1) = X $ VI(N) = V2
                    IF (X -XU) 50,51,51
                50  CONTINUE
20                  N = NMAX
                51  NO = N
                    IPR=MAXO(1,N/15)
                    PRINT 100, (I, XI(I), VI(I), I=1,N,IPR)
                100 FORMAT(*0       VI HAS BEEN (RE)CALCULATED*/(3(I10,  2G15.6)/))
25                  PRINT 200, N
                200 FORMAT(6X*ACTUAL NO. OF STEPS =*I4)
                C                                    . . . CALC. TIE,VI(XI)]
           1000     CT(1)=CT(4)=(1.0,0.0)
                    CT(2)=CT(3)=(0.0,0.0)
30                  CK2 = CSQRT(CMPLX(E-VI(1),0.0))
                    DO 10 I= 2,N
                    CK1 = CK2
                    CK2 = CSQRT(CMPLX(E-VI(I),0.0))
                    CKR=CK2/CK1
35                  CDELP= 0.5*CKR + 0.5
                    CDELM=CDELP-CKR
                    CKX=CK1*CMPLX(0.0,UNITS*XI(I))
                    CXPN=CEXP(CKX*CDELM)
                    CA(1)=CDELP/CXPN
40                  CA(4)=CDELP*CXPN
                    CXPN=CEXP(CKX*CDELP)
                    CA(3)=CDELM/CXPN
                    CA(2)=CDELM*CXPN
                    DO 10 J=1,2
45                  JP2 = J+2  $  CTO = CT(J)
                    CT(J) = CTO*CA(1) + CT(JP2)*CA(2)
                    CT(JP2) = CTO*CA(3) + CT(JP2)*CA(4)
                10  CONTINUE
                    T=CABS(CK2)/(SQRT(ABS(E-VI(1)))*CABS(CT(1))**2)
50                  RETURN
                20  T = 0.0  $  RETURN  $  END
```

Fig. A.1

TECHNICAL INFORMATION DIVISION
LAWRENCE BERKELEY LABORATORY
UNIVERSITY OF CALIFORNIA
BERKELEY, CALIFORNIA 94720